

A point to point response to the reviewers' comments

Thank you for the reviewers' comments on our manuscript entitled "Ozone affected by a succession of four landfall typhoons in the Yangtze River Delta, China: major processes and health impacts" (acp-2020-554). Those constructive comments are all valuable for revising and improving our manuscript, as well as the important guiding significance to our researches. We have studied those comments carefully and have made correction which we hope to meet with approval. Here are point to point responses (in blue colored). Accordingly, we also revised manuscript (in red colored).

Anonymous Referee #2:

General comments

A typhoon over the Western Pacific, as a large scale weather system during East Asian summer monsoon season, can significantly affect the tropospheric O₃ as well as air quality in a large region. The manuscript investigated the Landfall typhoon significantly affecting O₃ in the Yangtze River Delta (YRD) region, East China in respects of major processes and health impacts. This unique case study presented the interesting results on major processes of O₃ change driven by a succession of four landfall typhoons. This topic fits well into the scope of ACP.

Response: We would like to express our great appreciation to you for your encouragement.

Specific comments

The manuscript should be considered for publication only after making minor revisions as follows:

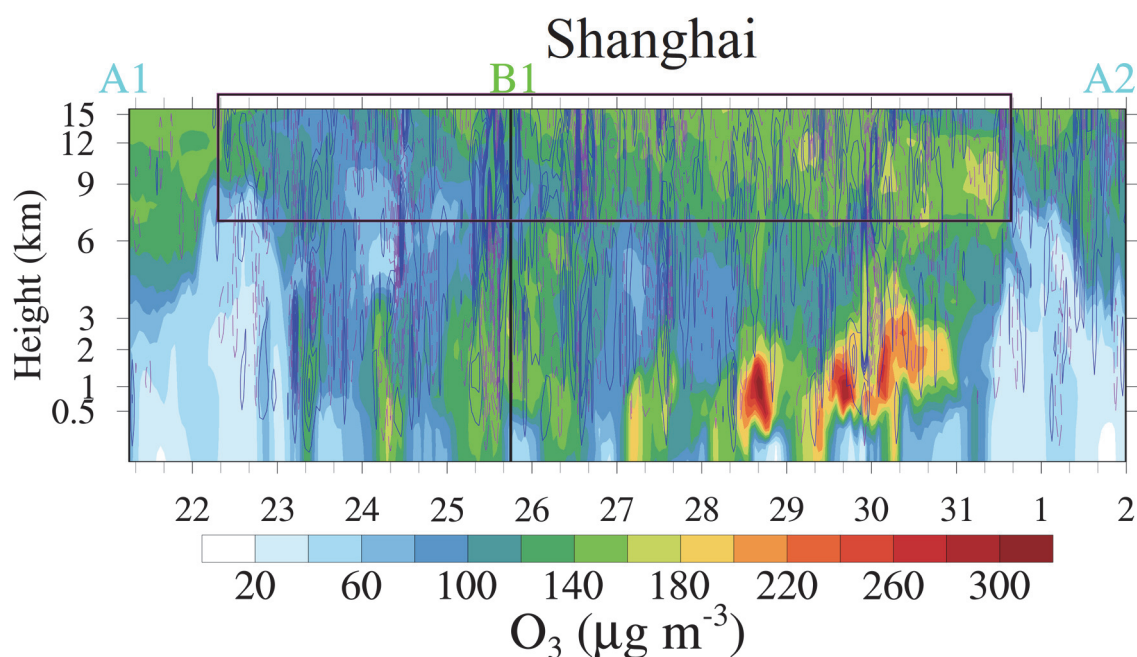
Response: We thank the reviewer for the constructive comments, which are really important to improving our manuscript. We have carefully revised our manuscript as shown below.

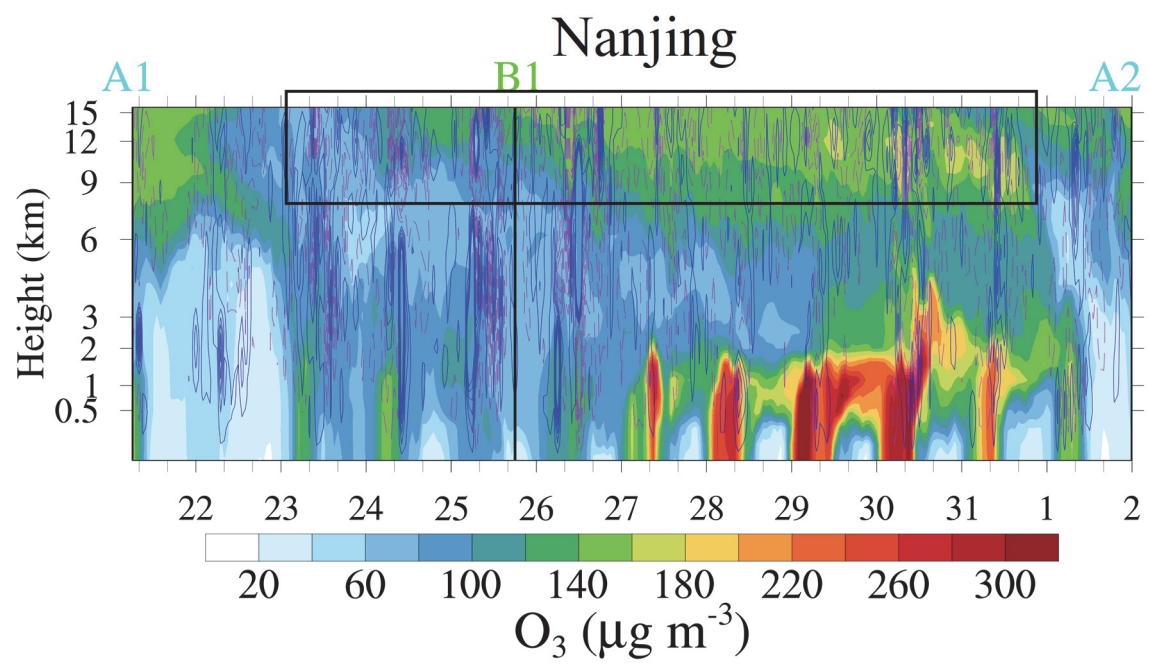
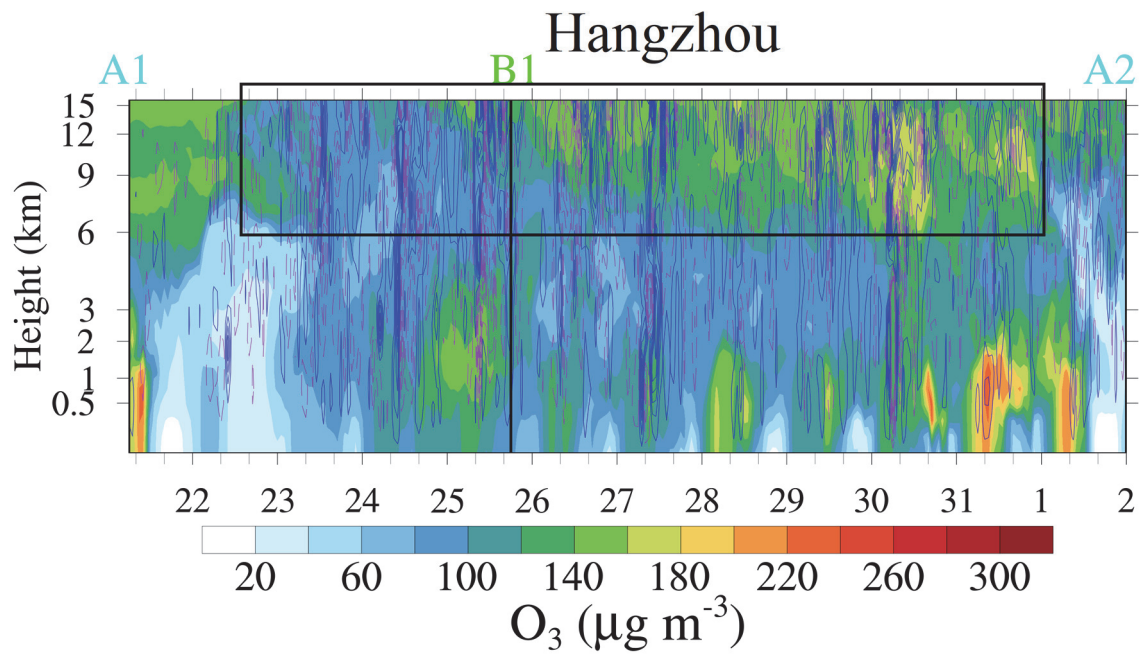
1. Please clarify the implication and limitation of this study for air quality change. A three-dimensional circulation of typhoon consists of the rotational air flow in the horizontal direction and the in-up-out-down overturning flow in the vertical direction, along which air mass near the surface can rise into thunderstorm clouds, outflowing at high levels in the UTLS and subsiding in the periphery. To better discuss the link with three-dimensional circulation of typhoon, please

reference this ACP paper: Jiang, Y. Zhao, T., Liu, J., et al. Why does surface ozone peak before a typhoon landing in southeast China? . Atmos. Chem. Phys., 2015, 15, 13331-13338.

Response: Thanks for the constructive comment and the important reference. We are deeply sorry that we ignored the three-dimensional structure of typhoons, especially the process of stratosphere-troposphere exchange of O₃. We have added this part, and reorganized the language in our revised manuscript. Please see lines 30-38 (Abstract), 410-422 (Sect. 3.3.2), 545-552 (Sect. 3.3.6), 634-641 (Sect. 4) and 728-730 (References) in the revised manuscript. Also, we have added a little implication to the discussion derived from the reference. Please see lines 564-565 (Sect. 3.3.6).

Figure R3 presents a fine map of temporal-vertical distribution of O₃ with vertical wind velocity over Shanghai, Hangzhou, Nanjing and Hefei between Typhoon Ampil and Typhoon Jongdari. Notably, O₃-poor air has penetrated into the stratosphere with the help of deep convection during typhoon, while O₃-rich air from the low stratosphere transported by downdrafts after typhoon. Combined with generated O₃ by photochemical reactions, high O₃ will appear in low troposphere. Moreover, the O₃ can remain at a high level in the residual at night, and can be transported to the surface by the second day. The transportation of O₃ in the upper layer plays an important role in the formation of O₃ pollution episodes on the surface.





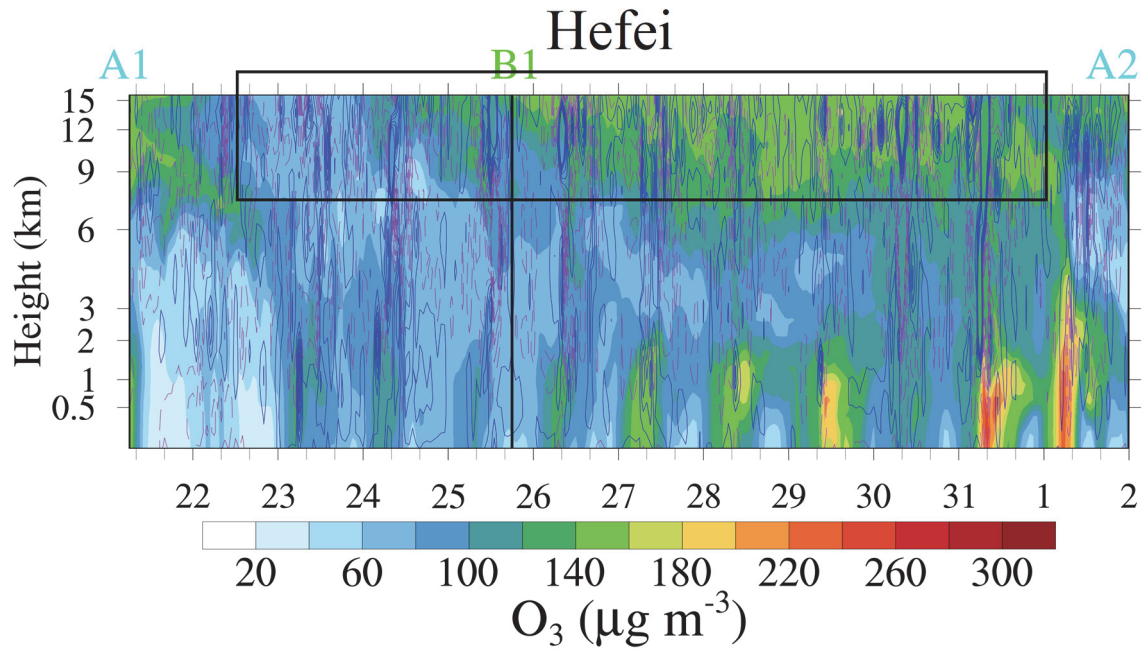


Figure R3: Temporal-vertical distribution of O_3 with vertical wind velocity over Shanghai, Hangzhou, Nanjing and Hefei. The dotted purple line and solid blue line indicate the negative wind speeds (downward airflows) and positive wind speeds (upward airflows), respectively. The time refers to UTC. The black box indicates the area of stratosphere-troposphere exchange (STE).

2. All Figs. (a) and (b) in Figs 6, 8 and 9 are too tiny to identify. Please improve the Figure presentations with better quality.

Response: Thanks for the constructive comment. In our revised manuscript, we have enhanced the quality of these figures with higher resolution and larger font size. Please see lines 431-433 (Fig. 6), 475-477 (Fig. 8), 502-504 (Fig. 9) and 522-524 (Fig. 10) in the revised manuscript.

3. Lines 485-487: this statement that “The YRD region, which features a typical subtropical monsoon climate, is strongly influenced by the western Pacific subtropical high in summer.” is incorrect or incomplete. The YRD, as a typical region of East Asian monsoon climate, is strongly influenced by typhoon activities over the Western Pacific.

Response: Thanks for the comment and correction. In this revising, the reviewer’s suggestion is followed. “The YRD region, which features a typical monsoon climate, is strongly influenced by

the western Pacific subtropical high in summer” has been changed to “The YRD, as a typical region of East Asian monsoon climate, is strongly influenced by typhoon activities over the Western Pacific.”. Please see lines 530-534 (Sect. 3.3.6) in the revised manuscript.

4. In synoptics, the western Pacific subtropical high and tropical cyclone (Typhoon) over western Pacific are two large scale weather systems in opposition to each other. Therefore, please remove “The subtropical high”, and “High temperature, southeast wind, downward airflow” from Fig. 11, also please correct the corresponding discussions.

Response: We appreciate this constructive comment. We are sorry that we did not carefully examine the synoptic meaning of the western Pacific subtropical high and tropical cyclone (Typhoon) in the last version, and we have changed both the schematic diagram and the corresponding discussions in the revised manuscript. Please see lines 44-45 (Abstract), 533-534 (Sect. 3.3.6), 557- 558 (Fig. 11) and 627 (Sect. 4) in the revised manuscript.

Ozone affected by a succession of four landfall typhoons in the Yangtze River Delta, China: major processes and health impacts

Chenchao Zhan ^{a,1}, Min Xie ^{a,*}, Chongwu Huang ^{a,1}, ~~Jane Liu~~ ^{b,c}, Tijian Wang ^a, ~~Jane Liu~~ ^{b,e}, Meng Xu ^d, Chaoqun Ma ^a, Jianwei Yu ^e, Yumeng Jiao ^f, Mengmeng Li ^a, Shu Li ^a, Bingliang Zhuang ^a, Ming Zhao ^a, Dongyang Nie ^a

^a School of Atmospheric Sciences, Joint Center for Atmospheric Radar Research of CMA/NJU, CMA-NJU Joint Laboratory for Climate Prediction Studies, Jiangsu Collaborative Innovation Center for Climate Change, Nanjing University, Nanjing 210023, China

^b College of Geographic Sciences, Fujian Normal University, 350007, Fuzhou, China

^c Department of Geography and Planning, University of Toronto, Toronto, Ontario, Canada

^d Jiangsu Provincial Climate Center, Nanjing 210009, China

^e Jiangsu Provincial Meteorological Observatory, Nanjing 210008, China

^f Department of Microbiology and Parasitology, Bengbu Medical College, Bengbu 233030, China

* Corresponding author. minxie@nju.edu.cn (M. Xie)

¹ The third author can be considered as the co-first author

Abstract: Landfall typhoon can significantly affect O₃ in the Yangtze River Delta (YRD) region. In this study, we investigate a unique case characterized by two multiday regional O₃ pollution episodes related to four successive landfall typhoons in the summer of 2018 in the YRD. The results show that O₃ pollution episodes mainly occurred during the period from the end of a typhoon ~~to and~~ the arrival of the next typhoon. The time when a moment that typhoon reached the 24-h warning line and the time when the last moment of typhoon ~~dies away~~ activity in the mainland China can be roughly regarded as time nodes. Meanwhile, the variations of O₃ was related to the track, duration and landing intensity of the typhoons. The impact of typhoons s on O₃ was like a wave superimposed on the background of high O₃ concentration in the YRD in summer. When a typhoon was near the 24-h warning line before it landed the coast line of the YRD, the prevailing wind originally from the ocean changed to from the inland, and transported lots of precursors from the polluted areas to the YRD. Under influences of the ~~With~~ typhoon, the low temperature, strong upward airflows, more

31 precipitation and wild wind ~~hindered occurrences of prevented~~ high O₃ episodes. After ~~the passing~~
32 ~~of the~~ typhoon, the air below the 700 hPa atmospheric layer was warm and dry, ~~and the downward~~
33 ~~airflows resumed. The low troposphere was filed with high concentration of O₃ due to O₃-rich air~~
34 ~~transported from the low stratosphere and strong photochemical reactions. which was conducive to~~
35 ~~the formation of O₃ from the abundance of precursors.~~ It is note-worthy that O₃ ~~was~~ mainly
36 generated in the middle of boundary layer (~ 1000 m) ~~instead of at the surface.~~ High O₃ remained
37 ~~in the residual layer at night, and would and be then~~ transported to the surface by downward airflows
38 or turbulences ~~by the second day~~. Moreover, O₃ can be accumulated and trapped on the ground due
39 to the poor diffusion conditions because the vertical diffusion and horizontal diffusion were
40 suppressed by downward airflows and light wind, respectively. The premature mortalities attributed
41 to O₃ exposure in the YRD during the study period ~~was~~ 194.0, more than the casualties caused
42 directly by the typhoons. This work ~~has enhanced~~ our understanding of how landfall typhoons
43 affect O₃ in the YRD ~~and thus can be useful, which can be helpful~~ to forecast ~~the~~ O₃ pollution
44 ~~synthetically impacted by the subtropical high and typhoon in regions strongly influenced by~~
45 ~~typhoon activities.~~

46 **Key Words:** ozone; landfall typhoon; the Yangtze River Delta region;

48 1 Introduction

49 The tropospheric ozone (O₃), which is formed by a series of complex photochemical reactions
50 between volatile organic compounds (VOCs) and nitrogen oxides (NO_x=NO+NO₂) in combination
51 with sunlight (Chameides and Walker, 1973; Xie et al., 2014), has received continuous attention due
52 to its negative impact on air quality (Chan and Yao, 2008; Monks et al., 2015), human health (Jerrett
53 et al., 2009), climate (Allen et al., 2012; IPCC, 2014) and biosphere (Dingenen et al., 2009).
54 Research on urban O₃ pollution can ~~be dated~~ back to the early 1950s, beginning with the Los Angeles
55 smog. In China, the photochemical smog, which is characterized by high level of O₃, was first
56 discovered in Xigu district of Lanzhou in 1970s (Tang et al., 1989). However, with the key
57 atmospheric environmental problem was coal-smoke pollution (such as acid rain) at that time (Wang
58 et al., 2019), little systematic research and coordinated O₃ monitoring were performed in China until
59 the mid-2000s (Wang et al., 2017).

60 Since the beginning of ~~the~~ 21st century, the complex air pollution, which is dominated by fine

61 particulate matter (PM_{2.5}, particles of 2.5 microns or less in aerodynamic diameter) and surface O₃,
62 has been ingrained in the megacities of China (Chan and Yao, 2008; Jin et al., 2016; Kan et al.,
63 2012). Air pollution has evolved into a political and economic concern in China. Due to ~~the~~
64 ~~strict~~~~drastic~~ air pollution control since 2013, particle pollution has been greatly reduced, appearing
65 a significantly decrease in sulfur dioxide (SO₂), NO_x and PM_{2.5}. However, the concentrations of O₃
66 and VOCs have ~~ved~~~~an~~ increased from 2013 to 2017 (Li et al., 2017), suggesting that more attention
67 should be paid to controlling O₃ and VOCs in the future. Overall, the causes of air pollution ~~and the~~
68 ~~control policies in China~~ are ~~remaining still a major~~ challenges ~~to confront in China~~, especially in
69 understanding the sources, transport and dispersion processes, and chemical formation mechanisms
70 of O₃ and its precursors (Ding et al., 2016; Guo et al., 2014; Huang et al., 2014).

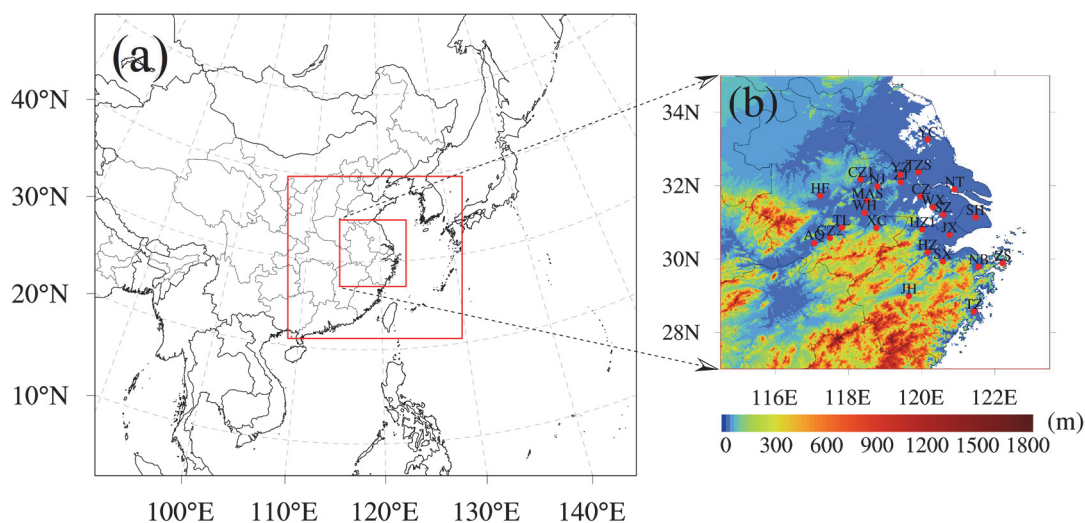
71 ~~A t~~Typhoon (tropical cyclone, TC) is one of the most ~~severe~~~~important factors of~~ natural
72 disasters in East Asia. Out of the total provinces in China, 10 coastal and 6 island provinces are
73 affected by typhoon induced disasters, with more than 250 million lives are affected (Liu et al.,
74 2009). The average number of typhoons making landfall in China is 9 each year, and those typhoons
75 usually inflict vast losses in human life and property due to the accompanied strong wind, torrential
76 rains and huge storm surges (Zhang et al., 2009; Zhao et al., 2012). Because of the long lifetime and
77 tremendous energy, typhoons ~~can~~~~has a~~ significantly ~~impact~~~~influence on~~ local atmospheric
78 conditions, and thereby can affect surface O₃ concentration through advection, diffusion, deposition
79 and other processes. The impact of typhoons on O₃ has attracted extensive attention in recent years
80 (Deng et al., 2019; Huang et al., 2005; [Jiang et al., 2015](#); Shu et al., 2016; Wang and Kwok, 2002;
81 Wei et al., 2016; Yang et al., 2012). For example, Deng et al. (2019) reported that high O₃ and high
82 aerosol concentrations (double high episodes) are likely to occur when the PRD is under the control
83 of ~~the~~ typhoon periphery and ~~the~~ subtropical high with strong downdrafts. Previous studies were
84 mainly in the southern China (including Hong Kong and Taiwan), where ~~are frequently affected by~~
85 typhoons ~~occur frequently~~. ~~Still~~~~However~~, research on the impact of landfall typhoons on O₃ is
86 ~~rather~~~~still~~ limited.

87 The Yangtze River Delta (YRD) region, being one of the most developed and densely
88 populated regions in China, is located on the western coast of the Pacific Ocean. With 3.7% of the
89 area and 16.0% of the population of China, the YRD contributed over 20% of the national total
90 Gross Domestic Product (GDP) in 2019. Due to the rapid economic development and high energy

91 consumption, this region ~~has been is~~ suffering from intense air pollution (Ding et al., 2013; Li et al.,
92 2019; Wang et al., 2015; Xie et al., 2016). In 2017, the 90th percentile of the maximum daily 8-hour
93 average (MDA8) O₃ concentration was 170 μg m⁻³, and 16 of the 26 cities (Figure 1b) in the YRD
94 failed to meet national standard (http://www.cnemc.cn/jcbg/zghjzkgb/201905/t20190529_704755.html). Therefore, it is ~~an urgent task~~ to investigate the spatiotemporal characteristic of O₃ as well as
95 its formation mechanisms in the YRD. Influenced by ~~the~~ monsoon weather, the warm and stagnation
96 conditions play an important role in the occurrence of high-level O₃ in summer (Li et al., 2018; Liao
97 et al., 2015; Lu et al., 2018; Zhao et al., 2010). Synoptic weather systems, such as typhoons and
98 cold fronts, ~~can also have~~ significantly ~~impacted effects on~~ O₃ in the YRD (Hu et al., 2013; Shu et al.,
99 2016). This work aims to reveal the main processes of landfall typhoon affecting surface O₃ in the
100 YRD, ~~hoping to~~ fill the knowledge gap and ~~thus provide scientific insight be helpful for~~
101 ~~effective making reasonable~~ pollution control measures.

103 In this study, we report a ~~typical outstanding~~ case observed in the YRD during the period from
104 16 July to 25 August, 2018, during which multiday episode of high O₃ occurred and was ~~found to~~
105 ~~be~~ related to four successive landfall typhoons. Base on the monitoring data and numerical
106 simulation, we ~~further~~ explore the impact of landfall typhoons on O₃ in the YRD, including the
107 major processes and health impacts. The following part of this paper is structured as the follows:
108 Section 2 gives a brief description of monitoring data, the analysis methods, and model
109 configurations. The results as well as the discussions are detailed in section 3. Section 4 summarizes
110 the main conclusions.

111



112

113 **Figure 1. The three nested modeling domains (a) in WRF, and the locations of 26 typical cities**
 114 **in the YRD with terrain elevation data (b). The cities in (b) include: Nanjing (NJ), Wuxi (WX),**
 115 **Changzhou (CZ), Suzhou (SZ), Nantong (NT), Yancheng (YC), Yangzhou (YZ), Zhenjiang (ZJ)**
 116 **and Taizhoushi (TZS) located in Jiangsu province; Hangzhou (HZ), Ningbo (NB), Jiaxing (JX),**
 117 **Huzhou (HZ1), Shaoxing (SX), Jinhua (JH), Zhoushan (ZS) and Taizhou (TZ) located in**
 118 **Zhejiang province; Hefei (HF), Wuhu (WH), Maanshan (MAS), Tongling (TL), Anqing (AQ),**
 119 **Chuzhou (CZ1), Chizhou (CZ2) and Xuancheng (XC) located in Anhui province; and the**
 120 **megacity Shanghai (SH). The terrain elevation data are available at**
 121 https://www.ngdc.noaa.gov/mgg/global/relief/ETOPO1/data/bedrock/cell_registered/netcdf/.

122

123 **2 Data and methods**

124 **2.1 Air quality data**

125 Surface air pollutants monitored by the China National Environmental Monitoring Center
 126 (CNMC) Network are used in this study. The nationwide observation network began operating in
 127 74 major cities in 2013, and it included 1597 nonrural sites covering 454 cities by 2017 (Lu et al.,
 128 2018). The monitoring data are strictly in accordance with the national monitoring regulations
 129 (<http://www.cnemc.cn/jcgf/dqhj/>), and can be acquired from the national urban air quality real-time
 130 publishing platform (<http://106.37.208.233:20035/>). Each monitoring site automatically measures
 131 hourly air pollutants (PM_{2.5}, PM₁₀, SO₂, NO₂, O₃ and CO), and the urban hourly pollutants are
 132 calculated by averaging the pollutants measured at all monitoring sites in that city. The MDA8 O₃

133 is calculated based on the hourly O₃ with more than 18-h measurements (Liao et al., 2017). Manual
134 inspection, including the identification and handling of invalid and lacking data, is performed
135 following previous studies (Xie et al., 2016; Shu et al., 2017; Zhan et al., 2019).

136 2.2 Surface and sounding meteorological data

137 With respect to surface observed meteorological data, stations at the three provincial capital
138 cities (~~Hefei~~, Nanjing ~~and~~, Hangzhou ~~and~~ Hefei) and the megacity Shanghai are selected, which
139 are ~~ZSOF (117.23°E, 31.87°N)~~, ZSNJ (~~32.00°N~~, 118.80°E, ~~32.00°N~~), ZSHC (~~30.23°N~~, 120.17°E,
140 ~~30.23°N~~), ~~ZSOF (31.87°N, 117.23°E)~~ and ZSPD (~~31.12°N~~, 121.77°E, ~~31.12°N~~), respectively. These
141 surface observations, including 2-m temperature, 10-m wind speed and direction and 2-m relative
142 humidity, are recorded hourly and can be obtained from the website of the University of Wyoming
143 (<http://weather.uwyo.edu/surface/>). ~~The precipitation data is not included in the dataset.~~

144 To verify the upper-air fields, the sounding observations at Shanghai (~~31.40°N~~, 121.46°E,
145 ~~31.40°N~~) and Nanjing (~~32.00°N~~, 118.80°E, ~~32.00°N~~) are used. These sounding observations
146 (pressure, temperature, relative humidity, wind direction and wind speed etc.) are also acquired from
147 the website of the University of Wyoming (<http://weather.uwyo.edu/upperair/sounding.html>), with
148 a time resolution of 12 h (00:00 and 12:00 UTC).

149 2.3 The best-track TC dataset

150 To capture the characteristics of landfall typhoons, the best-track TC dataset issued by the
151 China Meteorological Center (CMA) is considered due to its good performance on the landfall
152 typhoons in the mainland China (available at http://tcddata.typhoon.org.cn/zjljsjj_sm.html). The
153 dataset covers seasons from 1949 to the present, the region north of the equator and west of 180°E,
154 and is updated annually (Li and Hong, 2016; Ying et al., 2014). A wealth of information on typhoon
155 is recorded every 6h in the dataset, including location, minimum sea level pressure, etc. For landfall
156 typhoons, 24h before ~~their landing y land~~ and during their activities in the mainland China, the
157 ~~meteorological~~ data ~~are will be~~ recorded every 3h. Refer to the national standard for grade of tropical
158 cyclones (GB/T 19201-2006), the intensity category (IC) of tropical cyclones is ~~provided given~~ in
159 the dataset, which is based on the near surface maximum 2-min mean wind speed near the tropical
160 cyclone center, rang~~ing~~es from 1 to 6 (Table 1).

161

162 **Table 1. The intensity category of tropical cyclones**

Intensity category (IC)	The near surface maximum 2-min mean wind speed near the tropical cyclone center (m/s)	Beaufort scale
Tropical depression (IC=1)	10.8-17.1	6-7
Tropical storm (IC=2)	17.2-24.4	8-9
Severe tropical storm (IC=3)	24.5-32.6	10-11
Typhoon (IC=4)	32.7-41.4	12-13
Severe typhoon (IC=5)	41.5-50.9	14-15
Super typhoon (IC=6)	≥ 51.0	≥16

163

164 **2.4 Model description and configurations**

165 To simulate the high O₃ episodes over the YRD during the ~~period with~~ typhoon periods, the
166 WRF-CMAQ one-way coupled model is applied, which consists of WRF v3.6.1
167 (<https://www2.mmm.ucar.edu/wrf/users/>) developed by the United States National Center for
168 Atmospheric Research (NCAR) and CMAQ v5.0.2 (<https://github.com/USEPA/CMAQ/tree/5.0.2>)
169 developed by the United States Environmental Protection Agency (EPA).

170 WRF generates offline meteorological inputs for CMAQ with initial and boundary conditions
171 from the National Centers for Environmental Prediction (NCEP) global final analysis fields every
172 6 h at a spatial resolution of 1° × 1° (<https://rda.ucar.edu/datasets/ds083.2/>). Three nested domains
173 are used, with horizontal resolutions of 81, 27 and 9 km, and grids of 88 × 75, 85 × 79 and 97 × 97,
174 respectively (Figure 1a). There are 24 vertical sigma layers from surface to 100 hPa, with about 8
175 layers located below 1.5 km to resolve the boundary layer processes. Furthermore, the major
176 physical options for the dynamic parameterization in WRF are summarized in Table 2.

177

178 **Table 2. The domains and physical options for WRF in this study**

Items	Contents
Dimensions (x, y)	(88, 75), (85, 79), (97, 97)
Grid spacing (km)	81, 27, 9
Microphysics	WRF Single-Moment 5-class scheme (Hong et al., 2004)
Longwave radiation	RRTM scheme (Mlawer et al., 1997)

Shortwave radiation	Goddard scheme (Kim and Wang, 2011)
Surface layer	Moni-Obukhov scheme (Monin and Obukhov, 1954)
Land-surface layer	Noah land-surface model (Chen and Dudhia, 2001)
Planetary boundary layer	YSU scheme (Hong et al., 2006)
Cumulus parameterization	Grell-Devenyi ensemble scheme (Grell and Devenyi, 2002)

179

180 Since the horizontal domains of CMAQ are one grid smaller than WRF, all three nested
181 domains are adjusted automatically. The vertical layers of CMAQ are the same as WRF. The
182 Meteorology Chemistry Interface Processor (MCIP) can convert WRF outputs to the necessary
183 meteorological inputs for CMAQ. Moreover, the CB05 gas-phase mechanism with aqueous/cloud
184 chemistry is selected in the CMAQ configurations.

185 The anthropogenic emissions are from the Multi-resolution Emission Inventory for China
186 (MEIC) in 2016 with the resolution of 0.25° (<http://meicmodel.org/>), including anthropogenic
187 emissions from power generation, industry, agriculture, residential and transportation sectors. All
188 emission estimates are spatially allocated to the relevant grid cells based on the meteorological fields
189 obtained from WRF, and are temporally distributed on an hourly basis. The simulation starts from
190 00:00 UTC on 13 July to 00:00 UTC 27 August, with the first 72 h as spin-up time.

191 **2.5 Integrated process rate (IPR) analysis**

192 To quantify the contributions of individual processes ~~to~~ O₃ formation, the IPR analysis
193 provided in the CMAQ is utilized. The IPR analysis can illustrate the contributions to changes in
194 pollutant concentrations from seven different types of processes, including horizontal advection
195 (HADV), vertical advection (ZADV), horizontal diffusion (HDIF), vertical diffusion (VDIF), dry
196 deposition (DDEP), cloud processes with the aqueous chemistry (CLDS) and chemical reaction
197 process (CHEM), with a mass conservation adjustment at each model grid cell. The IPR analysis
198 has been widely applied to investigate regional air pollution (Fan et al., 2015; Li et al., 2012; Wang
199 et al., 2010). In this study, MADV is defined as the sum of HADV and ZADV, and TDIF is defined
200 as the sum of HDIF and VDIF.

201 **2.6 Model evaluation**

202 To evaluate the model performance, the simulation results in the innermost domain, including
203 O₃ concentration, air temperature at 2 m (T₂), relative humidity (RH), wind speed at 10 m (WS₁₀)

204 and wind direction at 10 m (WD₁₀), are examined against the hourly observations at the
 205 representative cities (Table 3). The statistical metrics, including correlation coefficient (R), root-
 206 mean-square error (RMSE) and normalized mean bias (NMB), are used ~~in this study~~. They are
 207 defined as follows:

$$208 \quad R = \frac{\sum_{i=1}^N (S_i - \bar{S})(O_i - \bar{O})}{\sqrt{\sum_{i=1}^N (S_i - \bar{S})^2} \sqrt{\sum_{i=1}^N (O_i - \bar{O})^2}}, \quad (3)$$

$$209 \quad RMSE = \sqrt{\frac{\sum_{i=1}^N (S_i - O_i)^2}{N}}, \quad (4)$$

$$210 \quad NMB = \frac{\sum_{i=1}^N (S_i - O_i)}{\sum_{i=1}^N O_i} \times 100\%, \quad (5)$$

211 where S_i and O_i are the simulations and observations, respectively. N is the total number of valid
 212 data. \bar{S} and \bar{O} are the average value of simulations and observations, respectively. In general, the
 213 model results are acceptable if the values of R , $RMSE$ and NMB are close to 1, 0 and 0, respectively
 214 (Li et al., 2017; Shu et al., 2016; Xie et al., 2016).

215 **2.7 Estimate of health impacts**

216 Previous studies showed that surface O_3 pollution can induce a series of adverse health
 217 problems impacts by causing from the incidence and mortality of respiratory diseases (Ghude et al.,
 218 2016; Jerrett et al., 2009; Lelieveld et al., 2015). To arouse more attention on the issue that O_3 can
 219 be significantly affected by typhoons in the YRD, we further estimate the premature mortality
 220 attributed to O_3 during the study period.

221 A standard damage function (Anenverg et al., 2010; Liu et al., 2018; Voorhees et al., 2014;
 222 WS/T 666-2019, Technical specifications for health risk assessment of ambient air pollution of
 223 China) is employed to quantify premature mortality due to O_3 exposure:

$$224 \quad \Delta M = y_0 \left(\frac{RR - 1}{RR} \right) Pop, \quad (1)$$

225 where ΔM is the excess mortalities attribute to O_3 exposure, y_0 is the baseline mortality rate, RR is
 226 relative risk and $(RR-1)/RR$ is the attributable fraction, and Pop is the exposed population. RR can

227 be calculated using the following relationship:

$$228 \quad RR = \exp(\beta(C - C_0)), \quad (2)$$

229 where β is the concentration-response factor, C is the exposure concentration and C_0 represents the
230 theoretical minimum-risk concentration.

231 In this study, the mortality rate for respiratory disease is obtained from China Health and
232 Family Planning Statistical Yearbook 2018 ([https://www.yearbookchina.com/navibooklist-](https://www.yearbookchina.com/navibooklist-n3018112802-1.html)
233 [n3018112802-1.html](https://www.yearbookchina.com/navibooklist-n3018112802-1.html)), which is 68.02/100000. The β is generated from Dong et al. (2016), that is
234 0.461%. The population data are obtained from the Bureau of Statistics of different cities in the
235 YRD. The C_0 is $70 \mu\text{g m}^{-3}$ for MDA8 O_3 given by the World Health Organization (WHO).

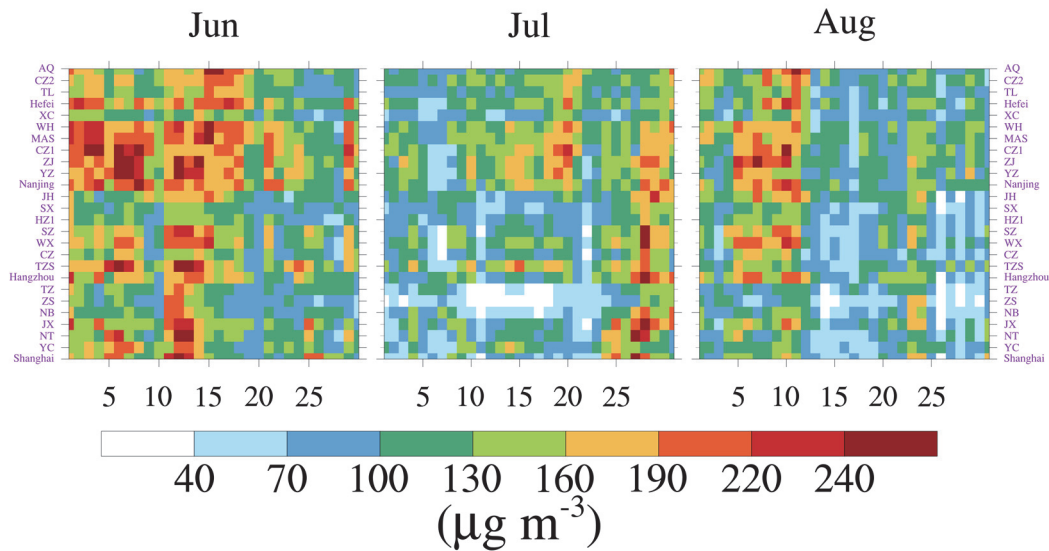
236

237 **3 Results and discussions**

238 **3.1 Characteristic of O_3 episodes**

239 In the midsummer ~~season~~, the warm sea surface (high temperature) is conducive to the
240 generation of typhoons (high O_3 concentration), ~~which~~ providing a good opportunity to investigate
241 the mechanism of typhoons affecting O_3 in the YRD. Figure 2 shows the MDA8 O_3 in the typical
242 26 cities of the YRD in summer of 2018. Actually, it is common for typhoons to affect O_3 in the
243 YRD during summer, and 2018 is special because there were 8 landfall typhoons and many of them
244 landed further north than in the normal years (see Supplement for details). O_3 concentration was
245 relatively ~~tended to be~~ high in June, and relatively low in July and August. The relatively low O_3
246 may be attributed to the maritime air masses transported by the Asian summer monsoon (Ding et
247 al., 2008; Xu et al., 2008). Nevertheless, we notice that there are two regional multiday O_3 pollution
248 episodes from 24 July to 11 August in the YRD, which means that about half of the cities in the
249 YRD exceed the national air quality standard (The national ambient air quality standard for MDA8
250 O_3 is $160 \mu\text{g m}^{-3}$ in China). The first multiday O_3 episodes appeared in most of the cities from 24
251 July to 2 August. The highest MDA8 O_3 concentration reached up to $264 \mu\text{g m}^{-3}$ on 27 July in
252 Ningbo (NB). O_3 pollution was even observed for 6 consecutive days from 27 July to 1 August in
253 Maanshan (MAS). Only two days later, regional O_3 pollution occurred in the YRD again from 5
254 August to 11 August.

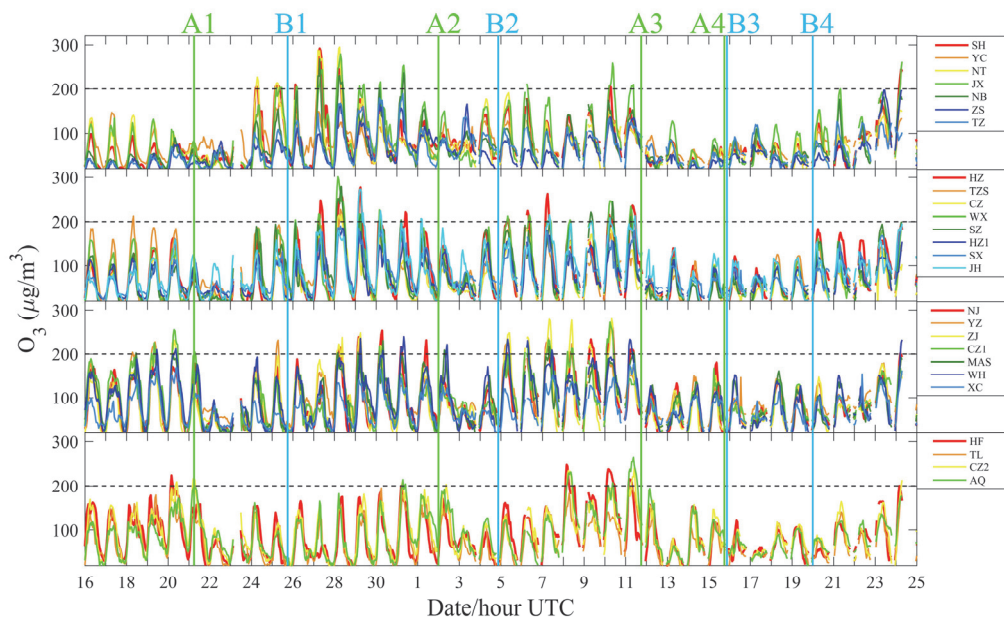
255



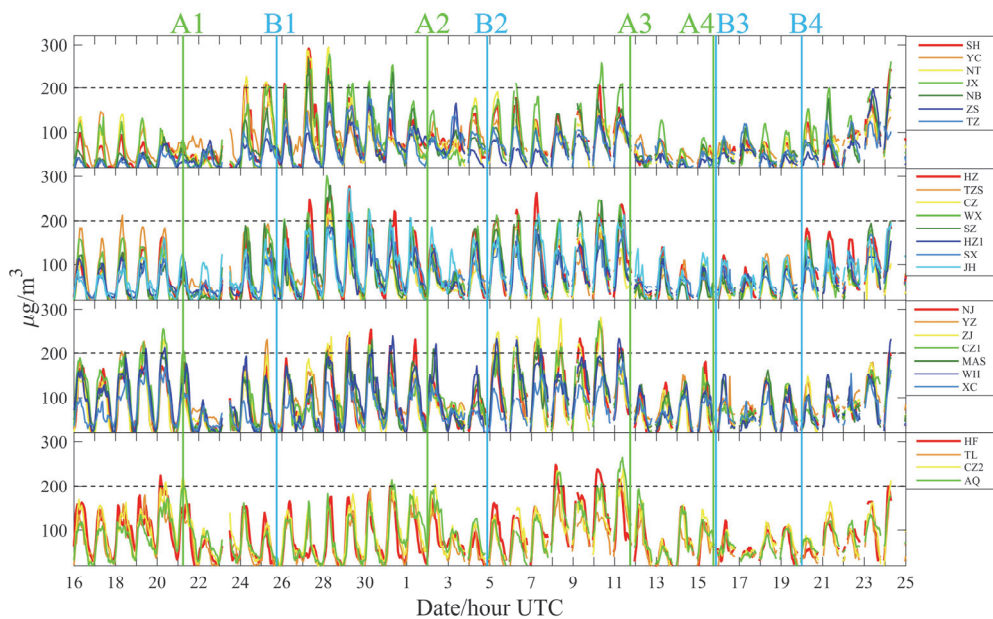
256
 257 **Figure 2. The MDA8 O₃ in 26 cities of the YRD in June (left panel), July (middle panel), and**
 258 **August (right panel) 2018summer of 2018. The national ambient air quality standard for**
 259 **MDA8 O₃ is 160 µg m⁻³ in China. These cities are sorted by longitude.**

260
 261 Figure 3 further shows diurnal variation of O₃ in all 26 cities of the YRD from 00:00 16 July
 262 to 00:00 25 August (throughout this paper the time refers to UTC, unless LST is specifically
 263 stated mentioned). Interestingly, O₃ pollution occurred earlier in cities near the coastline (e.g. large
 264 longitudes in °E, Figure 1b) rather than concurrently during the two multiday O₃ episodes. For
 265 example, from 24 July to 2 August, the first day that hourly O₃ concentration exceeded the national
 266 air quality standard (The national ambient air quality standard for hourly O₃ is 200 µg m⁻³ in China)
 267 in Shanghai, Hangzhou, Nanjing and Hefei was 24 July, 27 July, 28 July and 31 July, respectively.
 268 Thus, we classify the 26 cities in the YRD into four categories based on their longitudes, surrounding
 269 the four representative cities (Figure 4). The category I cities include SH, YC, NT, JX, NB, ZS and
 270 TZ. The category II cities include HZ, TZS, CZ, WX, SZ, HZ1, SX and JH, and the category III
 271 cities include NJ, YZ, ZJ, CZ1, MAS, WH and XC. Other cities are classified as the category IV
 272 cities, which are HF, TL, CZ2 and AQ. The first category cities are closest to the coastline, while
 273 the fourth category is the opposite.

274



275



276

277 **Figure 3. Diurnal variation of O₃ in all 26 cities of the YRD from 16 June to 25 August, 2018.**

278 **The grey dotted lines are the national ambient air quality standard for hourly O₃ (200 μg m⁻³)**

279 **in China. The letter A indicates the moment that the typhoon has reached the 24-h warning**

280 **line, and letter B indicates the last moment when the typhoon was active in the**

281 **mainland China. These time moments are acquired from the best-track TC dataset, depending**

282 **on the start and end times of the 3h densified observations. Coordinates 1, 2, 3, and 4 represent**

283 **Typhoon Ampil, Typhoon Jongdari, Typhoon Yagi, and Typhoon Rumbia, respectively. Note:**

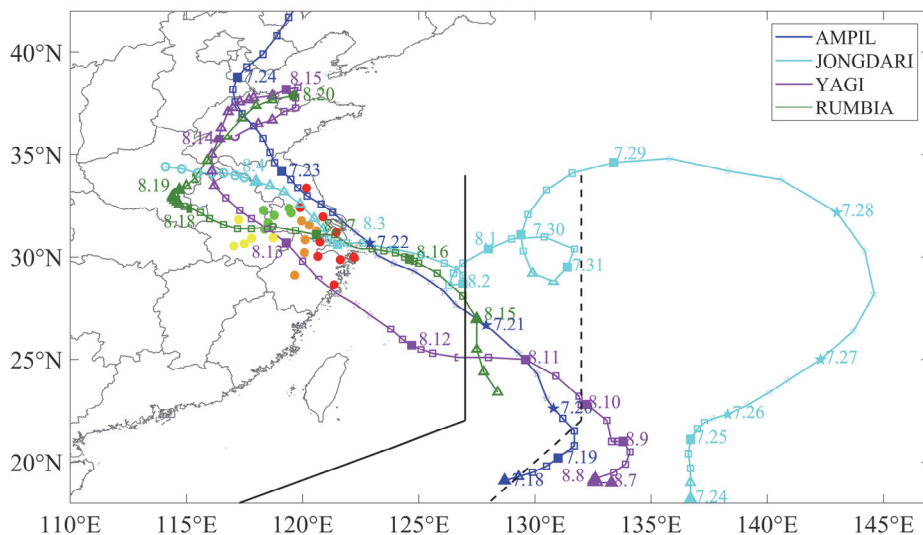
284 **these cities are sorted by longitude.**

285

286 3.2 Landfall typhoons and their effects

287 ~~For such~~ O₃ episodes with regional ~~and~~, long-lasting characteristics, may often be associated
288 with slow-moving synoptic weather systems. We find that the O₃ episodes coincided well with
289 ~~activities of~~ landfall typhoons ~~activities, showing in their~~ and ~~the~~ tracks and intensities ~~of typhoons~~
290 ~~are given~~ in Figure 4. Typhoon Ampil was first observed at 00:00 on 18 July, and landed in Shanghai
291 around 4:30 on 22 July with an intensity of severe tropical storm (IC=3). ~~While During the time of~~
292 Typhoon Ampil ~~remained active~~, Typhoon Jongdari generated over the western North Pacific at
293 12:00 on 23 July, and made landfall at the junction of Zhejiang province and Shanghai at 21:00 1
294 August. After Typhoon Jongdari, Typhoon Yagi generated at 00:00 7 August. At around 15:35 12
295 August, it landed in Zhejiang province and remained active in the mainland China until 21:00 15
296 August. Before the end of Typhoon Yagi, Typhoon Rumbia was observed over the western North
297 Pacific at 6:00 14 August. It finally landed in Shanghai at around 20:00 16 August, causing huge
298 economic losses.

299



300

301 **Figure 4. The track and intensity of Typhoon Ampil, Typhoon Jongdari, Typhoon Yagi, and**

302 **Typhoon Rumbia. The track is labeled with the date of the month and day (in month.day).**

303 **The circle, triangle, square and pentagram indicate the intensity category of tropical cyclones**

304 **is less than 1 (IC < 1), equal to 1 (IC = 1), equal to 2 (IC = 2), and not less than 3 (IC >= 3),**

305 **respectively. Black solid line and dotted line represent the 24-hour and 48-h warning line for**

306 **tropical cyclones, respectively. The colored solid points are the locations of cities in the YRD,**
307 **and different color represents different cities categories. Wherein, red, carrot, green and**
308 **yellow are category I, II, III and IV cities, respectively.**

309

310 To further understand the relationship between O₃ episodes and landfall typhoons, we mark the
311 critical moments of landfall typhoons in Figure 3. The letter A indicates the moment ~~when at~~
312 typhoons ~~has~~ve reached the 24-h warning line, and the letter B indicates the last moment of ~~that~~
313 typhoon ~~remains active~~activity in the mainland China. These moments are acquired from the best-
314 track TC dataset, depending on the start and the end time of the ~~densified-3h~~ observations.
315 Coordinates 1, 2, 3, and 4 represent Typhoon Ampil, Typhoon Jongdari, Typhoon Yagi, and Typhoon
316 Rumbia, respectively. As shown in Figure 3, O₃ exhibited a significant cycle during the study period.
317 That is, when the typhoon is close enough (near moments A1, A2, A3 and A4), the O₃ concentrations
318 decreased, but O₃ concentrations would increase as long as the typhoon was not active in the
319 mainland China (B1, B2 and B4) any more. This cycle would repeat if the next typhoon approached.
320 O₃ pollution was likely to occur during the period from the end of ~~at~~the typhoon to the arrival of the
321 next typhoon (B1A2 and B2A3) in the YRD.

322 Furthermore, we find that the variations of O₃ was related to the track, duration and landing
323 intensity of the typhoons. For example, during the B1A2 period when the O₃ pollution occurred, the
324 moments that hourly O₃ concentrations first exceed 200 µg m⁻³ in about half of cities of the
325 categories I, II, III and IV were 6:00 UTC (14:00 LST) 27 July, 6:00 UTC (14:00 LST) 28 July, 3:00
326 UTC (11:00 LST) 29 July and 6:00 UTC (14:00 LST) 31 July, respectively. This phenomenon also
327 suggests that O₃ pollution ~~first occurs-~~ in cities along the coastline~~in coastal region will be ahead~~
328 ~~of that in inland regions~~, which may be related to the track of typhoons (Figure 4). ~~Regarding~~As for
329 the impact of typhoon duration, the A4B3 period provided a good interpretation. While Typhoon
330 Yagi was still active in the mainland China, Typhoon Rumbia had reached the 24-hour warning line.
331 Hence, the O₃ remained a low level throughout the period (A3B4), which was quite different from
332 B1A2 and B2A3 period. Noted that the landing point and active path of Typhoon Ampil and
333 Typhoon Jongdari were very similar (Figure 4). However, the landing intensity of Typhoon Ampil
334 was severe tropical storm (IC = 3), and that of Typhoon Jongdari was tropical storm (IC = 2),
335 resulting in a difference in O₃ concentrations for Shanghai. Within 24 hours after Typhoon Ampil

(Jongdari) reached the 24-hour warning line, the average O₃ concentrations ~~reached~~ was 40.9 (80.1) μg m⁻³ in Shanghai. This is because that the stronger the typhoon landed, the gale (The 10-m wind speed near moment A1 was larger than that near moment A2 in Shanghai, Figure 7a) and precipitation accompanying the typhoon will be more effective in removing O₃.

3.3 Processes of O₃ pollution affecting by typhoons

To reveal the major processes of O₃ pollution episodes affected by landfall typhoons, ~~four~~ representative cities (Shanghai, Hangzhou, Nanjing and Hefei) one municipality and three provincial capital cities with different longitudes, including Shanghai (121.77°E, 31.12°N), Hangzhou (120.17°E, 30.23°N), Nanjing (118.80°E, 32.00°N) and Hefei (117.23°E, 31.87°N), are selected for further analysis – based on monitoring data and model results.

3.3.1 Evaluation of model performance

To evaluate the simulation performance, the hourly simulation results are compared with the measurements ~~from~~ during 00:00 16 July to 00:00 25 August. Table 3 presents the statistical metrics for selected variables, including temperature at 2 m (T₂), relative humidity (RH), wind speed at 10 m (WS₁₀), ~~and~~ wind direction at 10 m (WD₁₀), and surface O₃. T₂ is reasonably well simulated, with R values of 0.75, 0.77, 0.72 and 0.64 in Shanghai, Hangzhou, Nanjing and Hefei, respectively. Though our simulation underestimates T₂ to some ~~certain~~ extent, this ~~slightly~~ underestimation is acceptable because of ~~due to~~ the small RMSE (3.2, 2.7, 2.9 and 3.3) and NMB (-7.5%, -5.1%, -5.5% and -5.5%) values. As for RH, the simulation results are overestimated in all four cities, leading to the NMB values of 9.1%, 4.6%, 6.7% and 0.5% in Shanghai, Hangzhou, Nanjing and Hefei, respectively. With high R values (0.69, 0.65, 0.71 and 0.71) and relatively low RMSE values (12.4, 12.8, 12.1 and 10.8), the WRF simulates RH over the YRD quite well. The wind fields are closely related to the transport processes of air pollutants. The overestimation of WS₁₀ may partly be attributed to the unresolved terrain features by the default surface drag parameterization causing overestimation of wind speed in particular at low values (Jimenez and Dudhia, 2012; Li et al., 2017). With regards to WD₁₀, the simulation error is large based only on these statistical metrics. This is because that near-surface wind fields are deeply influenced by local underlying surface characteristics, and improving the urban canopy parameters might be useful (Liao et al., 2015; Xie et al., 2016). In term of O₃, the simulation results for ~~simulation results for~~ O₃ concentrations behave satisfactorily. R ~~is as high as~~ 0.55, 0.65, 0.66 and 0.54 for the simulations for ~~in~~ Shanghai, Hangzhou, Nanjing and

366 Hefei, respectively, while the NMB values are 5.8%, 16.4%, -6.2% and -5.3%, respectively.

367

368 **Table 3. Statistical metrics ~~infor~~ meteorological variables and O₃ concentration between the**
369 **observations and simulation~~se~~chemical-variables.**

City	Variable	\bar{O}	\bar{S}	R	RMSE	NMB
Shanghai	T ₂ (°C)	30.3	28.1	0.75	3.2	-7.5%
	RH (%)	75.0	81.8	0.69	12.4	9.1%
	WS ₁₀ (m s ⁻¹)	4.9	5.5	0.51	2.3	11.7%
	WD ₁₀ (°)	144.8	113.4	0.01	113.5	-22.9%
	O ₃ (μg m ⁻³)	74.3	76.5	0.55	45.3	5.8%
Hangzhou	T ₂ (°C)	30.3	28.8	0.77	2.7	-5.1%
	RH (%)	75.1	78.5	0.65	12.8	4.6%
	WS ₁₀ (m s ⁻¹)	3.3	4.7	0.32	2.7	32.5%
	WD ₁₀ (°)	155.0	114.7	-0.10	132.5	-27.8%
	O ₃ (μg m ⁻³)	81.7	91.3	0.65	49.8	16.4%
Nanjing	T ₂ (°C)	29.8	28.1	0.72	2.9	-5.5%
	RH (%)	77.4	82.6	0.71	12.1	6.7%
	WS ₁₀ (m s ⁻¹)	3.1	5.0	0.39	3.0	63.8%
	WD ₁₀ (°)	132.8	115.6	0.21	102.7	-15.0%
	O ₃ (μg m ⁻³)	87.6	79.8	0.66	46.7	-6.2%
Hefei	T ₂ (°C)	29.3	27.7	0.64	3.3	-5.5%
	RH (%)	81.1	81.5	0.71	10.8	0.5%
	WS ₁₀ (m s ⁻¹)	3.2	3.2	0.37	2.2	2.9%
	WD ₁₀ (°)	147.0	128.6	0.04	136.7	-13.3%
	O ₃ (μg m ⁻³)	87.3	80.3	0.54	45.0	-5.3%

370 *Note.* R exceeds 0.1 to reach statistically significant at 99.9% confident level. \bar{O} and \bar{S} are the
371 average values of the observations and simulations, respectively.

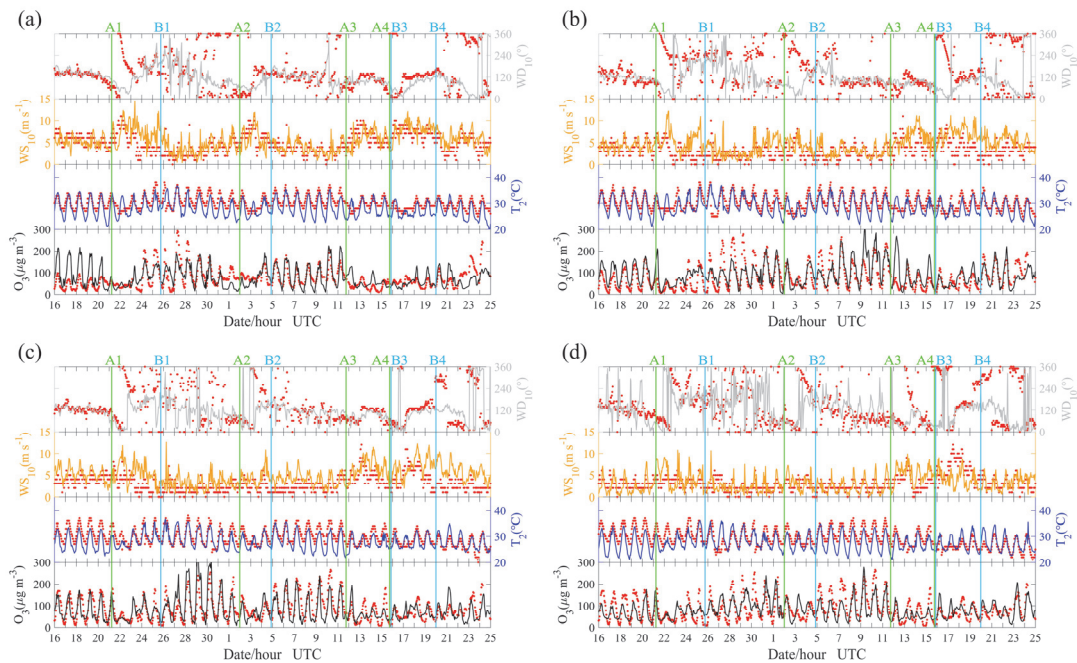
372

373 Figure 5 further shows hourly variations of O₃, T₂, WS₁₀ and WD₁₀ for measurements and
374 simulations in four representative cities. The simulations effectively reproduce the diurnal variation
375 of O₃, T₂ and WS₁₀, confirming the reliability of the simulation results. Moreover, the model well
376 captures the shift in wind direction during the study period. Thus, the overall model performance in
377 simulating~~for~~ wind fields is acceptable. In summary, the simulations results can capture and
378 reproduce the major meteorological characteristics and O₃ evolution during of the O₃ episodes, and
379 thus including the meteorological conditions and evolution of O₃, which can provide valuable

380 insights into the formation of the O₃ episodes.

381

382



383

384 **Figure 5. Hourly variations of O₃, T₂, WS₁₀ and WD₁₀ infor measurements (red dots) and**
385 **simulation (colored lines) in (a) Shanghai, (b) Hangzhou, (c) Nanjing and (d) Hefei.**

386

387 3.3.2 Shanghai in category I cities

388 In theis study period, Shanghai was usually one of the first cities affected by landfall typhoons.

389 We can see a multiday episode of O₃ during the period of 24-28 July, with a maximum of hourly O₃

390 up to 292 μg m⁻³ at 27 July (Figure 6a). The high O₃ concentrations together with high primary

391 pollutants (CO and NO₂) suggest a strong photochemical O₃ production under the condition of high

392 temperature (The daily maximum temperature can reach 35 °C) during this period, and the weak

393 wind may play a significant role in the accumulation of surface O₃. The increase of the primary

394 pollutants may be related to the wind shifta change in wind direction from southeast to southwest

395 causing by Typhoon Ampil (A1 in Figure 6a, -A1 and A1B1 in Figure 7), resulting in air masses

396 originally from the ocean had become inlandwhich originally brought airmass from the ocean,

397 shifted to from inland. Interestingly, PM_{2.5} also showed good correlation with O₃ and primary

398 pollutants, especially for NO₂ during this period. This indicates that a high level of oxidizability can

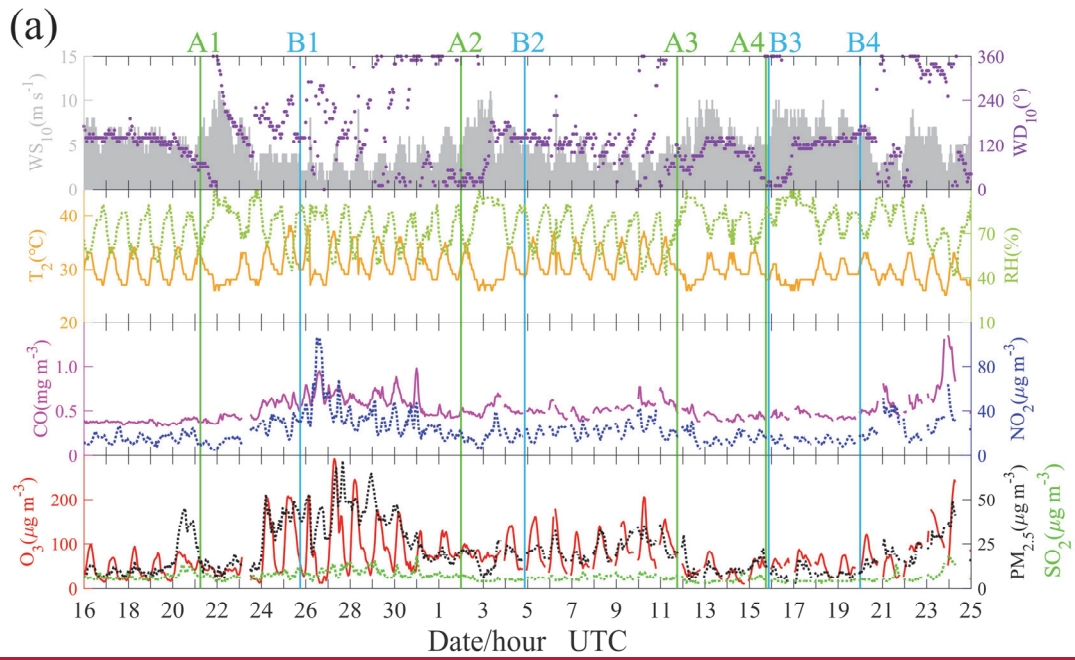
399 promote the formation of secondary particles (Kamens et al., 1999; Khoder, 2002). From the results

400 of process analysis (Figure 6b), the major contributions to surface O₃ were TDIF, CHEM and DDEP

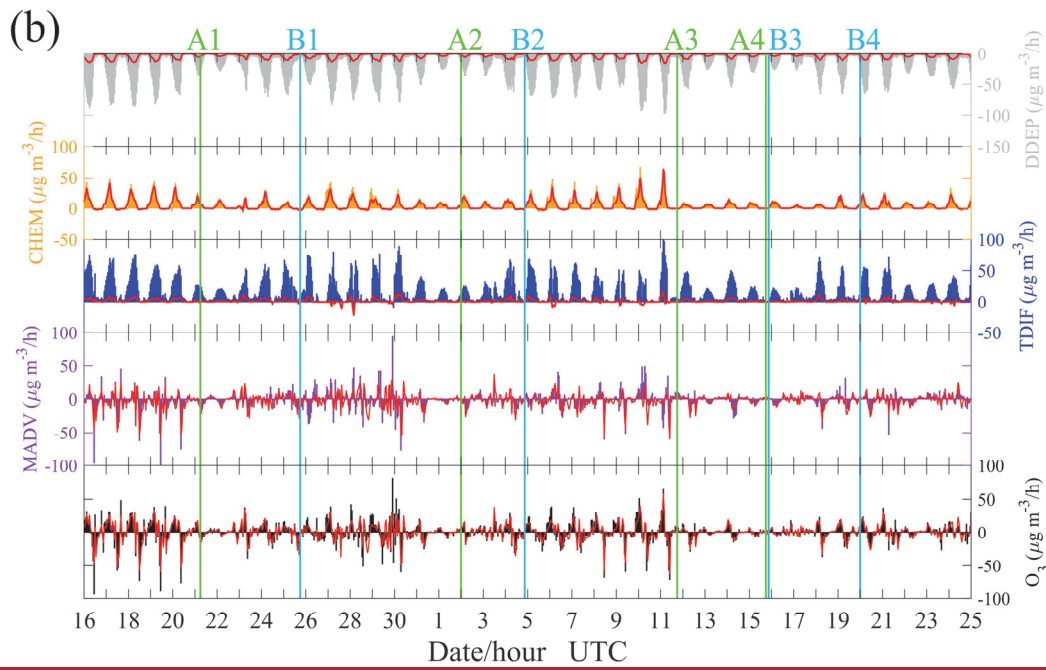
401 due to the small net contribution of MADV. TDIF had a considerable positive contribution while
402 DDEP did the opposite, suggesting that high surface O₃ may be sourced from the upper layer via
403 TDIF process, and be removed via DDEP process. However, for the whole boundary layer, which
404 is defined as the layer less than 1500 m in this study, ~~it was~~ the balance was between CHEM and
405 DDEP instead TDIF and DDEP. Thus, TDIF was likely to play the role of “transport” from the upper
406 layer to surface. Figure 6c further shows the temporal-vertical distribution of O₃ with vertical wind
407 velocity. The downward airflows ~~were~~ prevailed over Shanghai until 23 July, which are induced by
408 the subtropical high. Then, strong upward airflows appeared as Typhoon Ampil arrived, and high
409 level of O₃ disappeared. Around 27 July, the downward airflows gradually resumed and high level
410 of O₃ occurred. The downward airflows are critical because they can not only inhibit the vertical
411 transport of O₃ but also transport high-level O₃ to the surface. The high-level O₃ in the troposphere
412 mainly comes from two sources. One is that O₃-rich air from the low stratosphere transported by
413 the downdrafts in large-scale typhoon circulation (Jiang et al., 2015). The other is that O₃ produced
414 by photochemical reactions during the day. It is note-worthy that ~~the high value center of O₃~~
415 ~~appeared near the altitude of 1 km instead of near surface, indicting~~ high photochemical production
416 efficiency of O₃ occurred in the middle boundary layer instead of at the surface. Moreover, most of
417 the O₃ remained in the residual layer at night, while surface O₃ concentration was much lower due
418 to NO_x titration. By the second day, high O₃ in the residual layer was transported to the surface by
419 the downward airflows as air in the boundary layer is gradually mixed. Combined with the newly
420 generated O₃, a high concentration of O₃ would eventually appear on the surface. ~~The downward~~
421 ~~airflows can not only inhibit the vertical transport of O₃ but also transport high-level O₃ to the~~
422 ~~surface, causing the episodes of surface O₃.~~

423 As shown in Figure 7, O₃ pollution tends to occur during the period from the end of ~~the~~
424 typhoon to the arrival of the next typhoon (B1A2 and B2A3) in the YRD. To reveal this phenomenon,
425 we compare these two periods (B1A2 and B2A3) with their previous periods (A1B1 and A2B2)
426 using the skew-T log-P diagram (Figure 6d and 6e). It is found that the atmospheric conditions of
427 B1A2 (B2A3) were hotter and drier than A1B1 (A2B2) below 700 hPa in Shanghai, and wind speed
428 is smaller in B1A2 (B2A3). Those changes in atmospheric conditions after typhoon will be
429 conducive to the generation of high O₃ concentration in Shanghai.

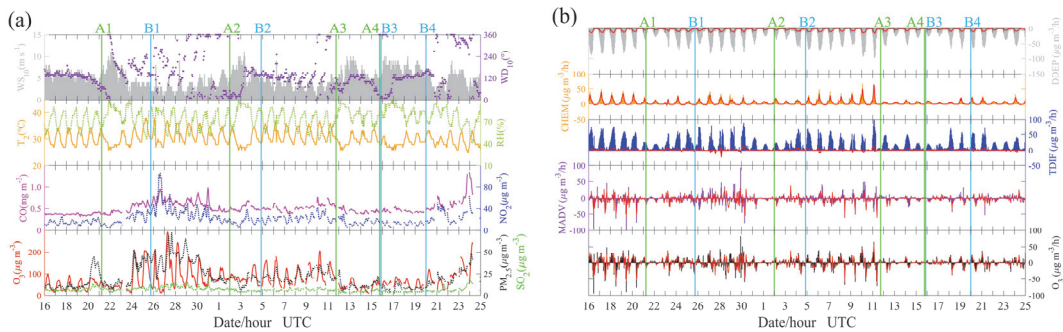
430



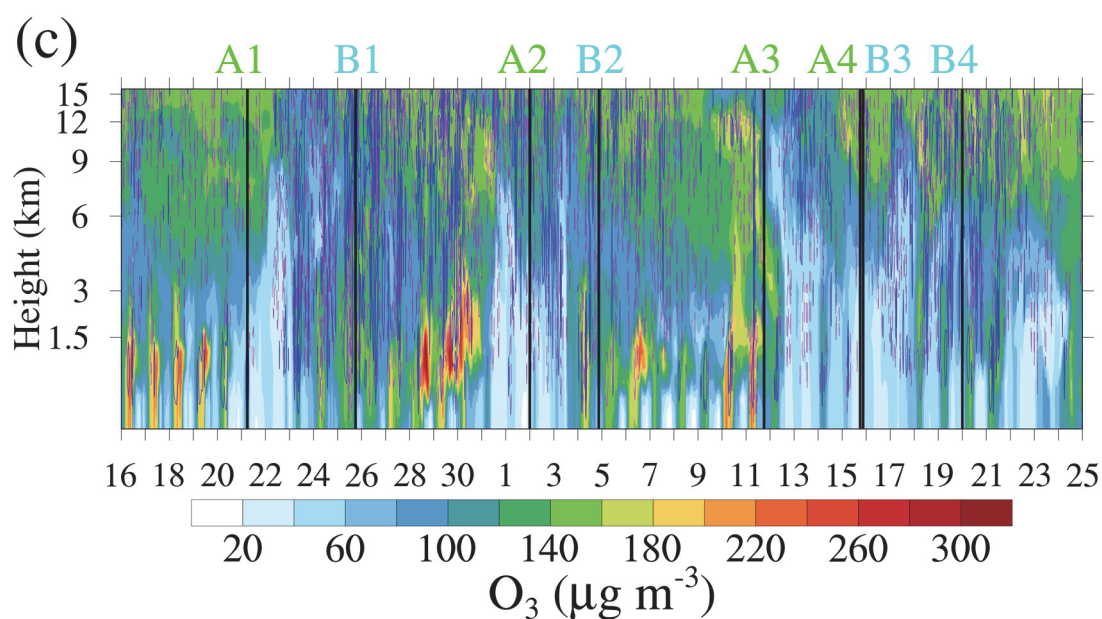
431



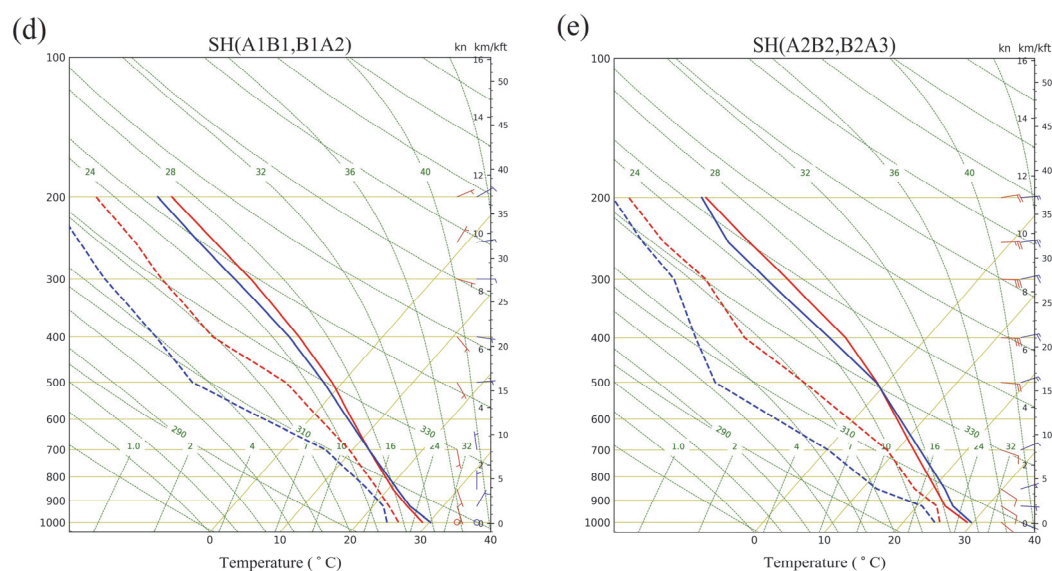
432



433



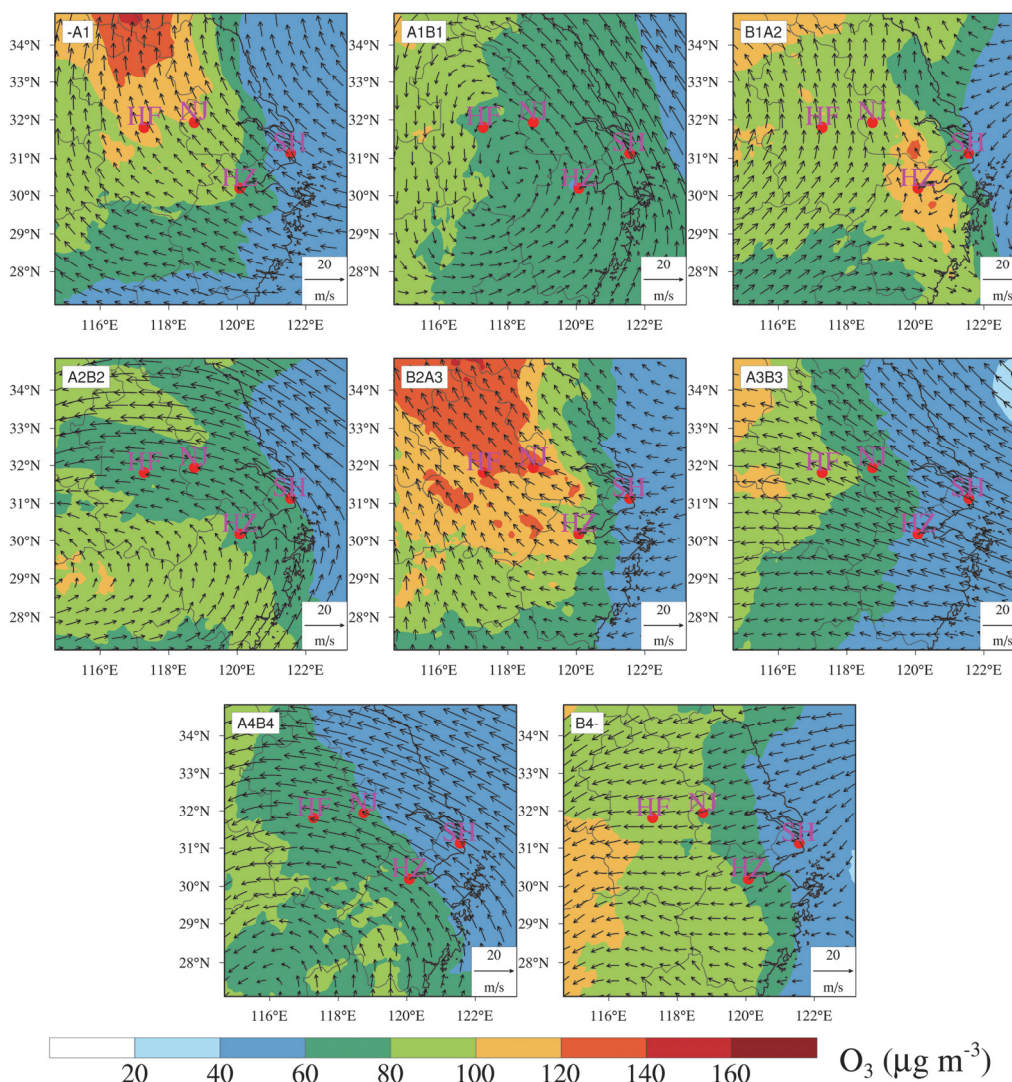
434



435

436 **Figure 6. (a) Time series of air pollutants (O_3 , $PM_{2.5}$, SO_2 , CO and NO_2) and meteorological**
 437 **factors (T_2 , RH , WS_{10} and WD_{10}) in Shanghai. (b) Individual processes contribution to net O_3**
 438 **density at Shanghai. O_3 is the net increase, MADV is the sum of horizontal advection (HADV)**
 439 **and vertical advection (ZADV), TDIF is the sum of horizontal diffusion (HDIF) and vertical**
 440 **diffusion (VDIF), CHEM is the chemical reaction process, and DDEP is the dry deposition**
 441 **process. The color histograms indicate the results for the layer near the surface, while the solid**
 442 **red lines indicate the average results for all layers below 1500 m. (c) Temporal-vertical**
 443 **distribution of O_3 with vertical wind velocity over Shanghai. The dotted purple line and solid**
 444 **blue line indicate the negative wind speeds (downward airflows) and positive wind speeds**

445 (upward airflows), respectively. (d) The skew-T log-P diagram at Shanghai. The average
 446 results of period A1B1 and B1A2 are shown in red and blue, respectively. (e) Same as (d), but
 447 for the average results of period A2B2 and B2A3.
 448



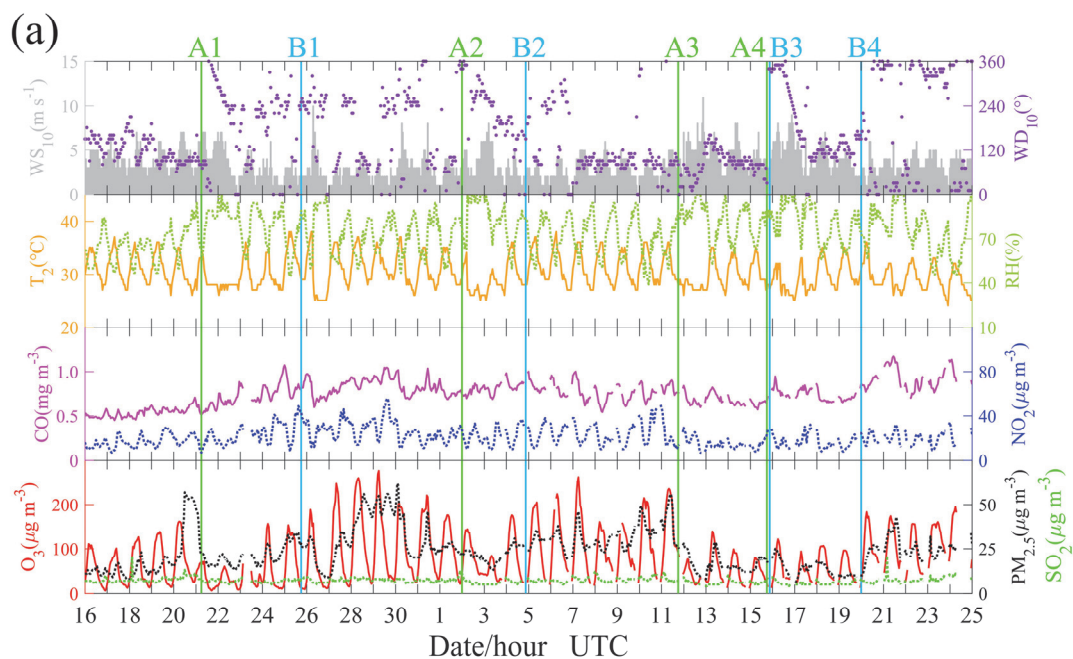
449
 450 **Figure 7. Spatial distribution of surface O₃ overlaid with wind fields at 850 hPa over the YRD.**
 451 **-A1, A1B1, B1A2, A2B2, B2A3, A3B3, A4B4, B4-** are the average results from the beginning
 452 **to A1, A1 to B1, B1 to A2, A2 to B2, B2 to A3, A3 to B3, A4 to B4, and B4 to the end, respectively.**
 453 **Details can be found in Figure 4.**

454
 455 **3.3.3 Hangzhou in category II cities**

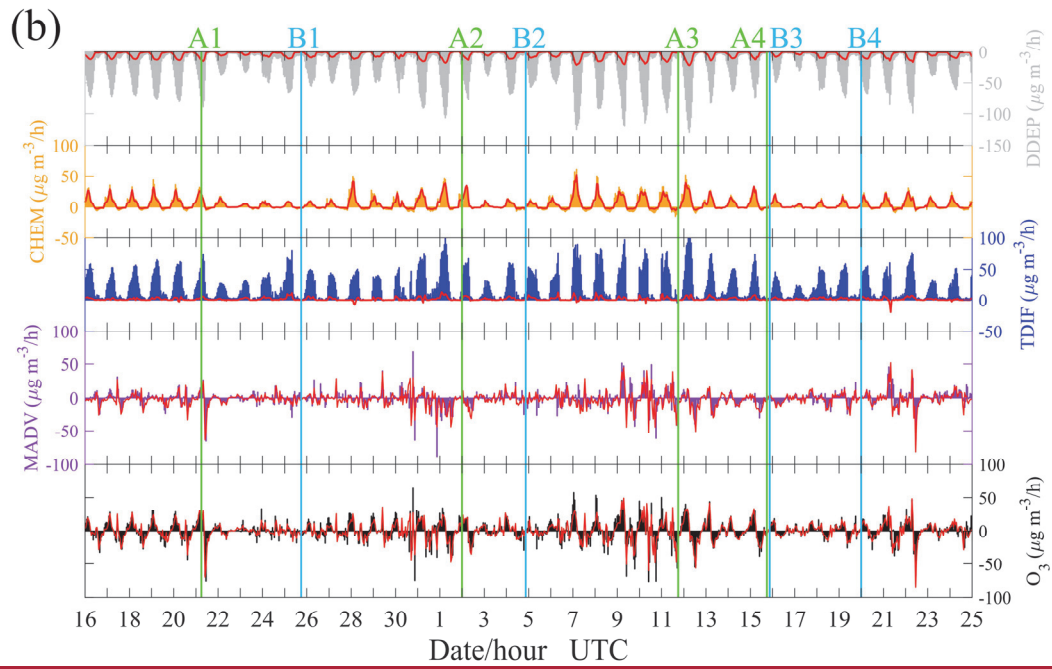
456 Figure 8 presents the ~~case inresults for~~ Hangzhou. It shows that high O₃ concentrations
 457 occurred on 27-31 July and 5-7 August, which may also be related to the strong photochemical

458 production of O₃ under the abundance of precursors (Figure 8a) and poor diffusion conditions due
 459 to the light wind (B1A2 and B2A3 in Figure 7). Figure 8a further shows that high O₃ was often
 460 associated with an increase in CO but the NO₂ concentrations usually remained at the same level.
 461 This phenomenon indicates a VOCs-limited regime in this city since CO usually have good
 462 correlation with VOCs and can play a similar role as VOCs in the photochemical production of O₃
 463 (Atkinson, 2000; Ding et al., 2013). In fact, O₃ in other representative cities (Shanghai, Nanjing and
 464 Hefei) also showed a better correlation with CO than NO₂. Though Hangzhou is close to Shanghai,
 465 there is a significant difference of wind fields over these two cities. Starting from the arrival of
 466 Typhoon Ampil (A1). The wind direction in Hangzhou did not change back to southeast until a few
 467 days later after Typhoon Jongdari dissipated (B2). During this period (A1B2), the frequent
 468 southwest wind may be the reason for high CO concentrations in Hangzhou. In addition, the chaotic
 469 wind field during period B1A2 (B1A2 in Figure 7) may lead to the light wind in Hangzhou. With
 470 respect to the simulation results, the model simulated the variation of O₃ but failed to capture the O₃
 471 peaks (e.g., the peak values on 27-31 July), which may be related to the strong upward airflows
 472 (Figure 8c) that inhibited the accumulation of O₃ (Figure 8b). This further illustrates that downward
 473 airflows may be an important factor for O₃ episodes in this case.

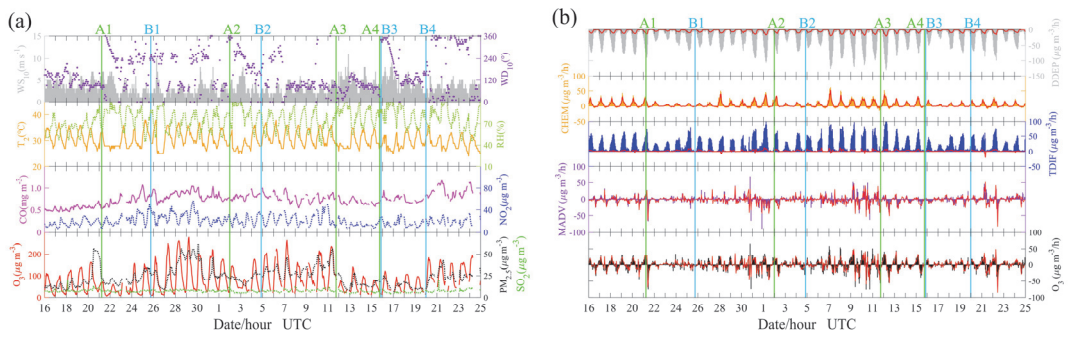
474



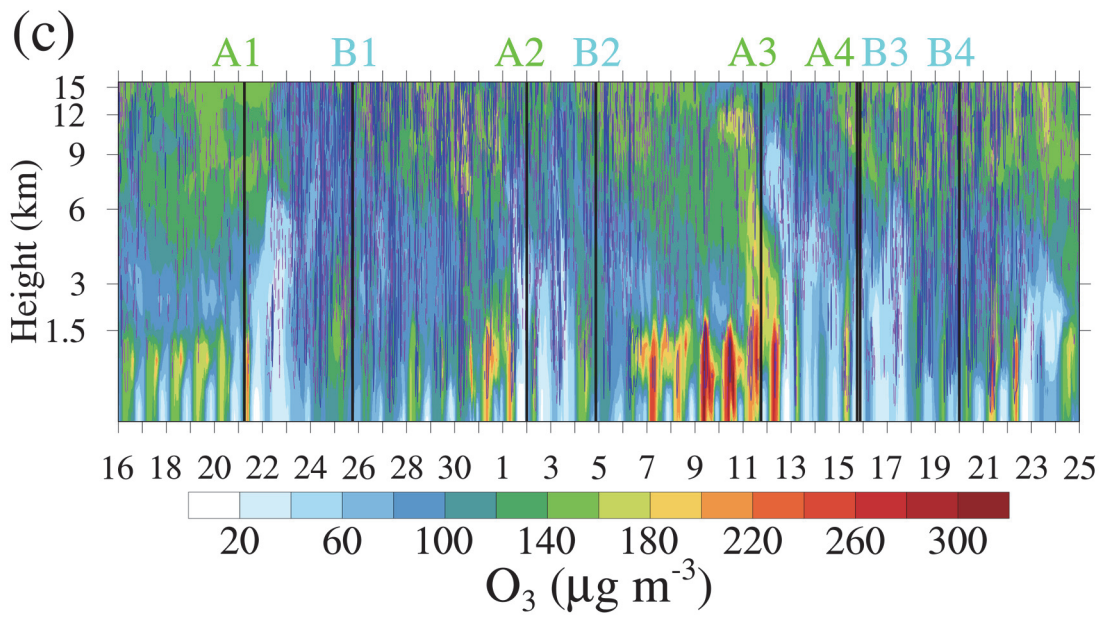
475



476



477



478

479

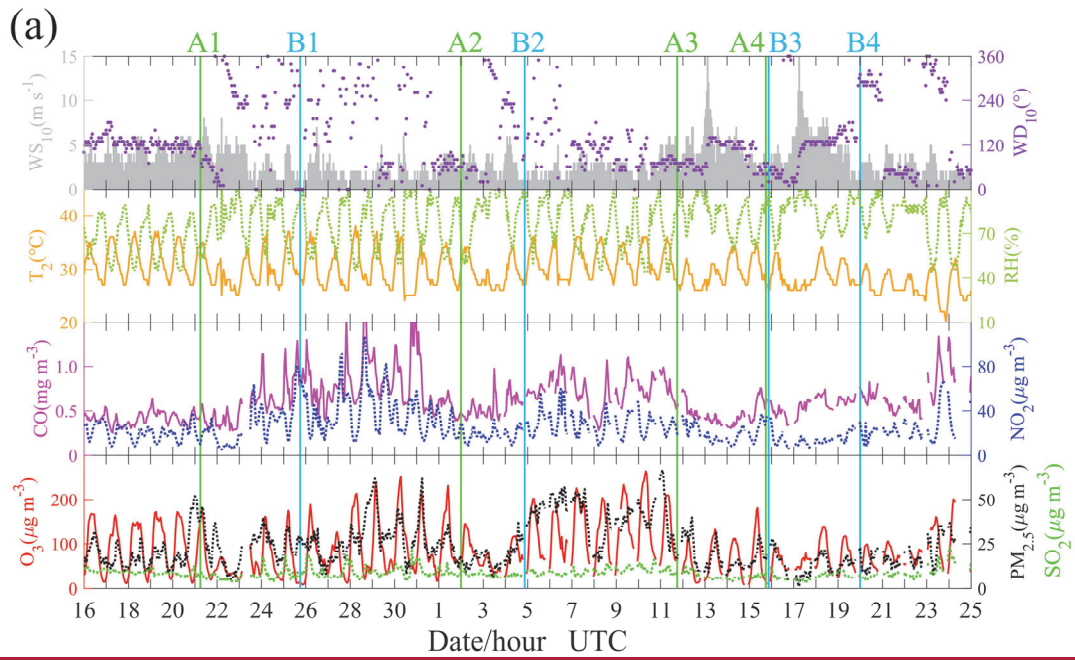
Figure 8. Same as Figure 6 (a)-(c), but for Hangzhou.

480

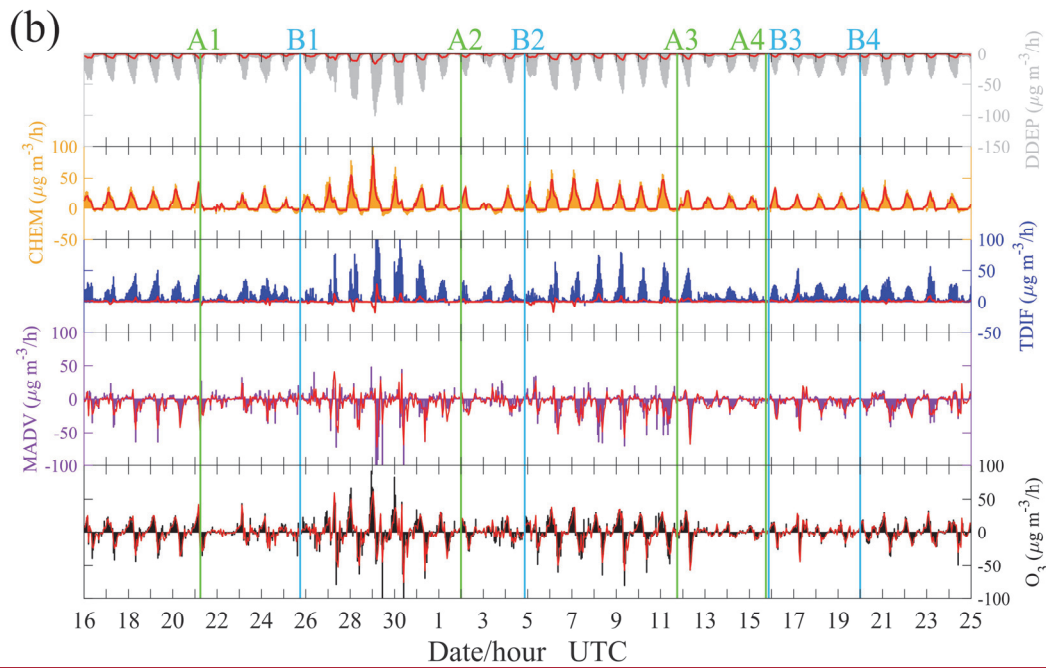
481 3.3.4 Nanjing in category III cities

482 ~~In~~As for Nanjing, the O₃ episodes ~~with~~ exceeded ~~the~~ ~~anee~~ ~~of~~ national air quality standards
483 ~~was~~ere observed on 28 July to 1 August and 7-11 August. These O₃ episodes were characterized by
484 abundant O₃ precursors under the condition of high temperature. Furthermore, light wind (B1A2
485 and B2A3 in Figure 7) and downward airflows (Figure 9c) also contributed greatly to the occurrence
486 of O₃ pollution, ~~resulting from a mechanism similar to~~~~with the similar mechanism as~~ that ~~for~~
487 Shanghai and Hangzhou. As early as on 22 July, the wind direction in Nanjing ~~had~~ changed from
488 southeast to southwest ~~because of the arrival of~~~~affected by~~ Typhoon Ampil, and thus the
489 concentrations of the main primary pollutants (CO, NO₂ and SO₂) increased (Figure 9a). However,
490 high-level O₃ episodes did not occur until 28 July even though the maximum temperature did not
491 change significantly during 24-31 July. The “obstacle” ~~for enhancing O₃ level~~~~of the O₃ episodes~~
492 may be the precipitation ~~caused~~~~ing~~ by the strong upward airflows during 23-26 July (Figure 9c). As
493 shown in Figure 9b, high surface O₃ concentration during the pollution episodes is the result of
494 TDIF and CHEM processes, and is lost through DDEP and MADV processes. ~~Regarding~~~~With~~
495 ~~respect to the~~ vertical structure of atmospheric, B1A2 (B2A3) was also hotter and drier than A1B1
496 (A2B2) below 700 hPa in Nanjing (Figure 9d and 9e). ~~These consequences, similar to those in~~~~The~~
497 ~~similar results as~~ Shanghai, further confirm that high O₃ concentrations in a region are more likely
498 to occur during the period from the end of ~~an exciting~~~~the~~ typhoon to the arrival of the next typhoon
499 (B1A2 and B2A3) than during the period when ~~at~~the typhoon approaches and is active in the
500 ~~region~~~~mainland China~~ (A1B1 and A2B2).

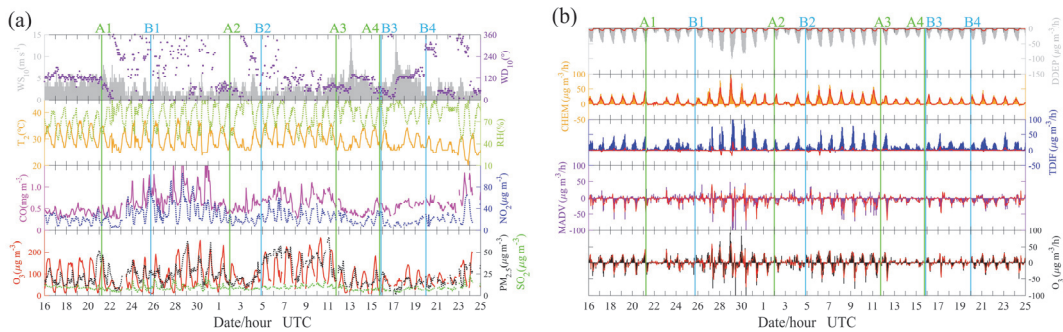
501



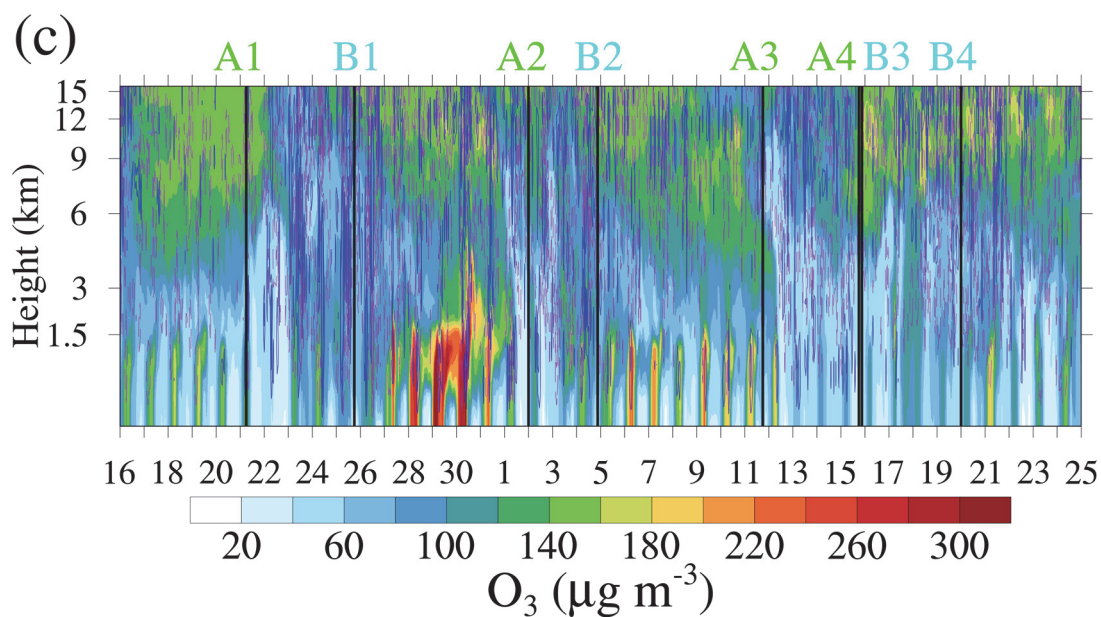
502



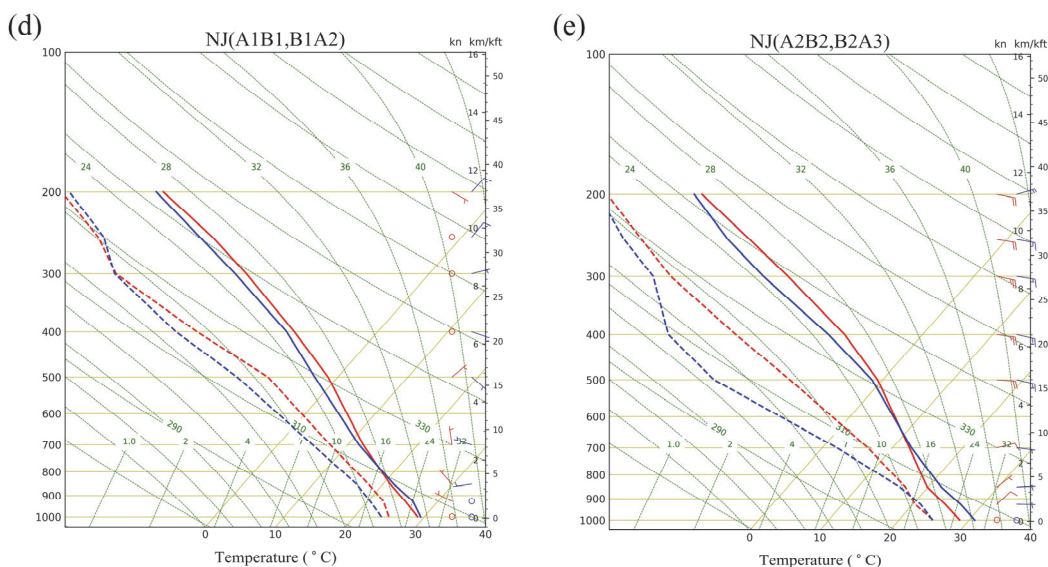
503



504



505



506

507 **Figure 9. Same as Figure 6, but for Nanjing.**

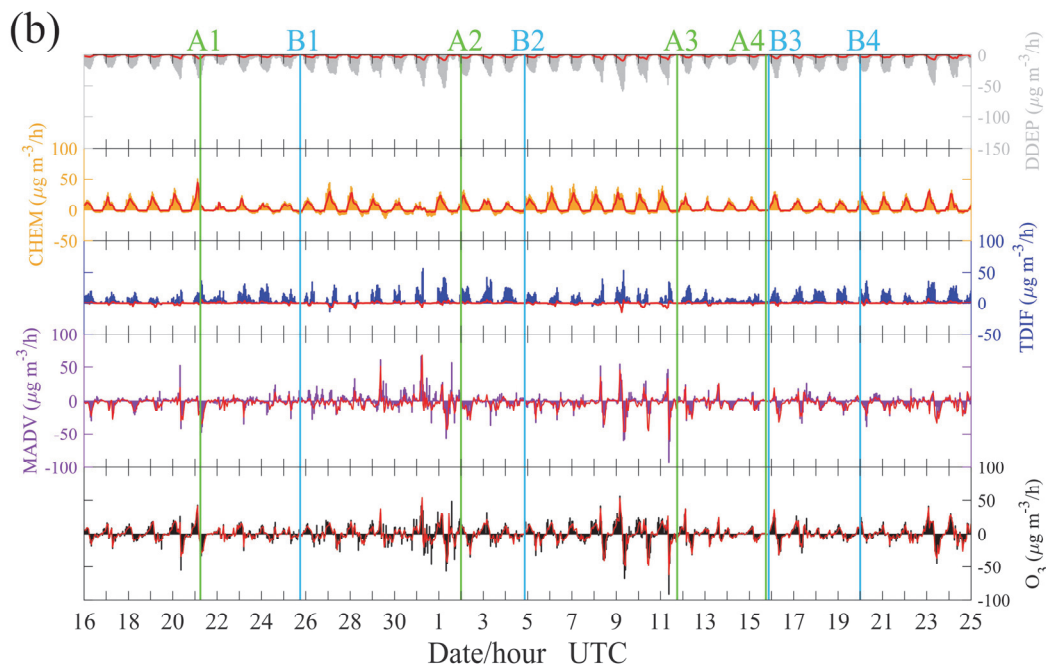
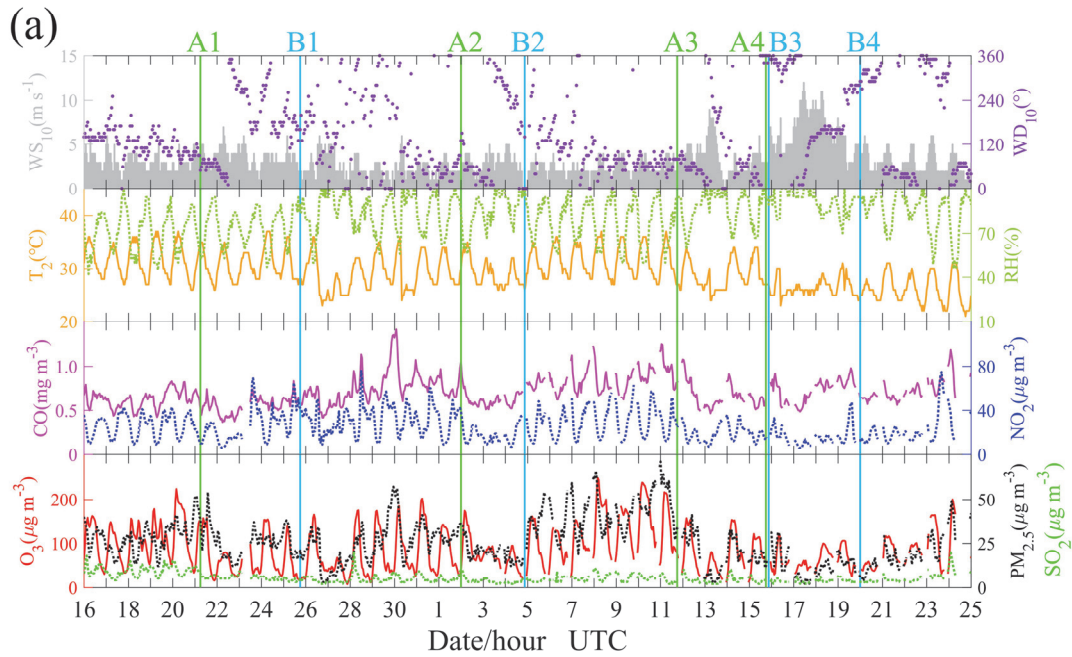
508

509 3.3.5 Hefei in category IV cities

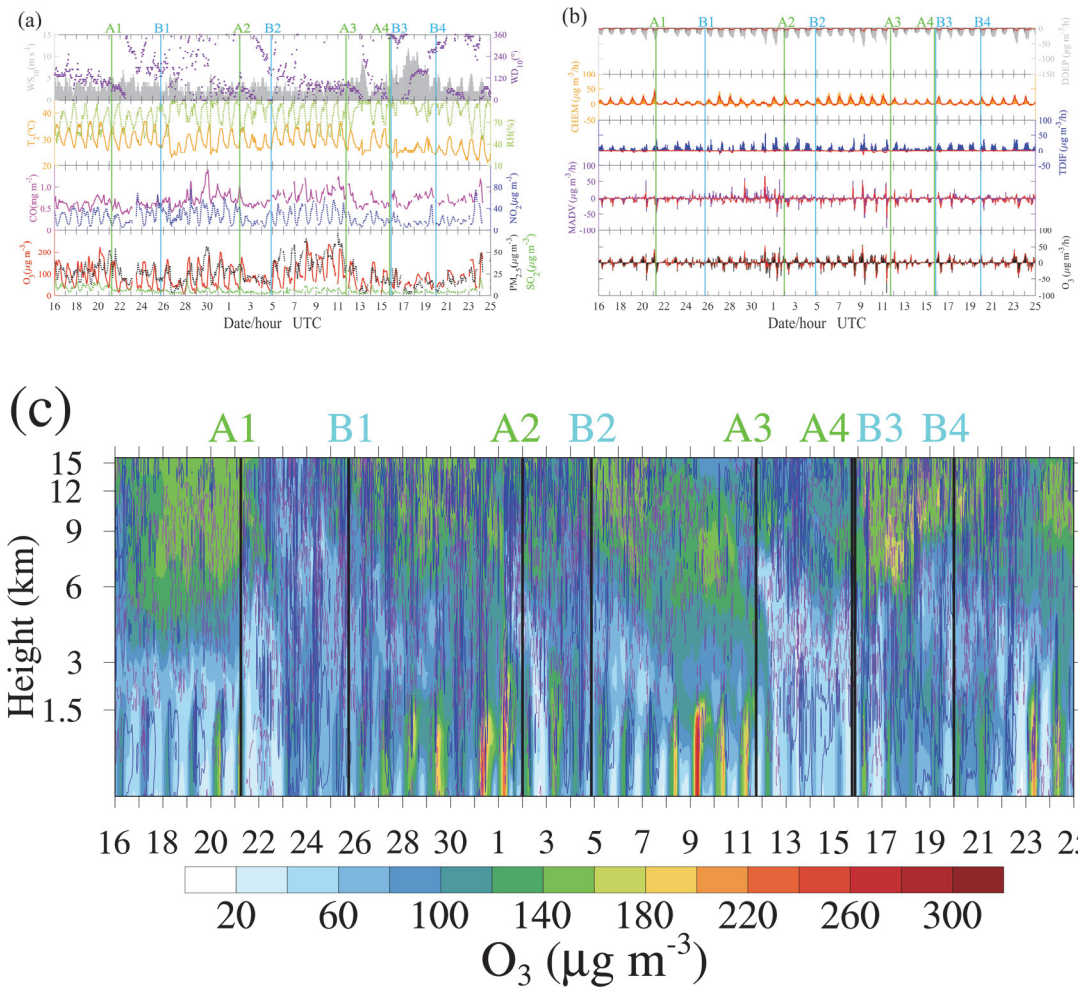
510 Hefei is the city farthest from the coast among the four representative cities, and O₃ pollution
 511 occurred on 31 July and 8-11 August. We ~~can~~ also find the phenomenon that the precursors
 512 concentrations had an increase once the wind direction changed from southeast to southwest (Figure
 513 10a). During B1A2 and B2A3, the concentrations of the main precursors of O₃ washed a high level.
 514 However, high O₃ concentration was mainly found in B2A3, and not in B1A2. This may be related
 515 to the relatively low temperature during B1A2 (Figure 10a), which is not conducive to

516 photochemical production of O₃ (Figure 10b). As shown in Figure 10c, there were distinct upward
 517 airflows within the boundary layer, which may be related to urban effect (e.g., urban heat islands).
 518 These upward airflows within the boundary layer help mix the air, resulting in a uniform distribution
 519 of O₃ in the vertical direction. However, the downward airflows can still inhibit the vertical diffusion
 520 of O₃, and O₃ tends to be trapped within the boundary layer.

521



524



525

526 **Figure 10.** Same as Figure 6 (a)-(c), but for Hefei.

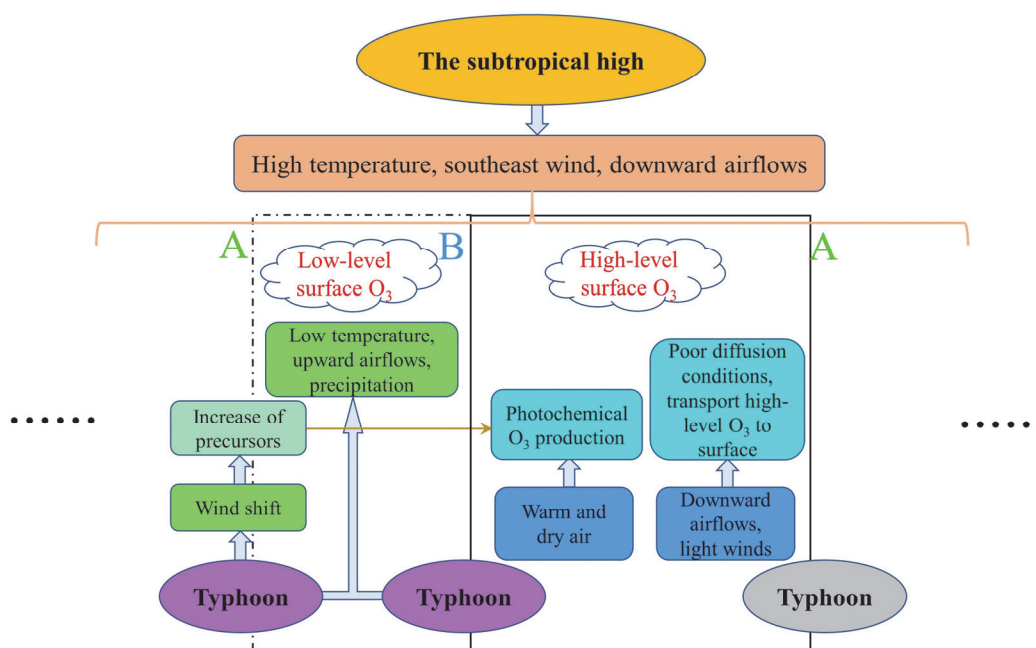
527

528 3.3.6 A schematic diagram of major processes

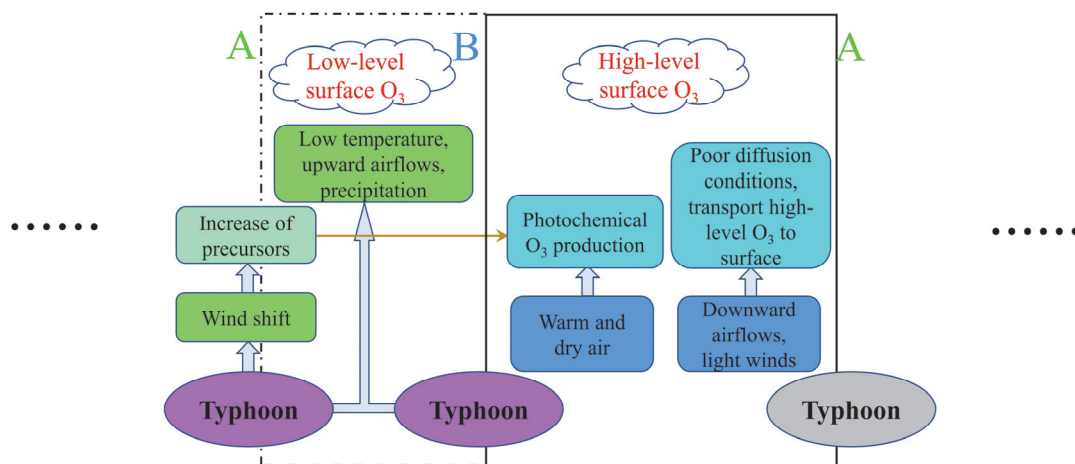
529 Although the processes of landfall typhoon affecting O₃ varied from city to city, the major
 530 processes have many similarities and can be summarized as a schematic diagram in Figure 11. The
 531 YRD region, as a typical region of East Asian monsoon climate, is strongly influenced by typhoon
 532 activities over the Western Pacific ~~The YRD region, which features a typical subtropical monsoon~~
 533 ~~climate, is strongly influenced by the western Pacific subtropical high in summer. Dominated by the~~
 534 ~~subtropical high~~ In summer, the meteorological conditions of high temperature and downward
 535 airflows combined with high levels of precursors due to the huge energy consumption ~~tend to form~~
 536 ~~high O₃ concentrations in this region~~ are all favorable to O₃ accumulation in the region. However,
 537 powerful systems like typhoon can break this state. For typhoons that may land in the YRD, by the
 538 time they approach the 24-hour warning line, the prevailing southeast wind in the YRD will change

539 to southwest wind, which can transport lots of precursors from inland to the YRD. The change in
 540 wind direction depends on the track of the typhoon and the geographical location of cities, and often
 541 appears first in cities along the coastline~~eastal~~ region. With influence of a typhoon, the low
 542 temperature, precipitation (upward airflows) and wild wind ~~will~~ prevent high O₃ and PM_{2.5} episodes
 543 from forming. Moreover, the effect of removing pollutants is related to the intensity of typhoon
 544 landing, but some of the main precursors of O₃ are still at a high level due to foreign sources
 545 superposed with local emissions. After the passing of typhoons, the atmosphere returns to a warm
 546 and dry state (even more so than before), and the downward airflows resumed. The troposphere is
 547 then flooded with high O₃ due to two main sources. One is that O₃-rich air transported from the low
 548 stratosphere by the downward airflows, and the other is that O₃ produced by strong photochemical
 549 reactions begin to produce O₃ under the abundance of precursors. O₃ is mainly generated inside the
 550 boundary layer (~1000 m) instead of at the surface. The high-level O₃ can remain in the residual
 551 layer at night, and be then transported to the surface by downward airflows or turbulent mixing by
 552 the second day. At the same time, the wind readjusts to southeast and wind speed is light, resulting
 553 in poor diffusion conditions. The downward airflows and light wind obstruct the vertical and
 554 horizontal diffusion of O₃, leaving O₃ trapped on the ground. The thermal-dynamic effects result in
 555 high-level surface O₃ in the YRD.

556



557



558
 559 **Figure 11. A schematic diagram of major processes that summertime O₃ is affected by landfall**
 560 **typhoons in the YRD. The letter A indicates the moment that the typhoon has reached the 24-**
 561 **h warning line, and letter B indicates the last moment when typhoon remains active**
 562 **in the mainland China.**

563
 564 Typhoon can exert an enormous impact on energy transports and air mass in the troposphere
 565 as well as redistribution of pollutants. Though ~~In fact~~, most typhoons generated over the western
 566 North Pacific will not land in China, or they are more likely to land in the South China rather than
 567 the YRD. In our previous study (Shu et al., 2016), the typhoon did not land in the YRD, but the
 568 processes ~~related to~~ high-level O₃ formation may be ~~the same~~ common. That is, the processes
 569 shown in the ~~open box enclosed by dashed lines~~ dashed box in Figure 11, which are unique to landfall
 570 typhoons, while the processes ~~inside the box enclosed by solid lines~~ in the solid box can be found
 571 ~~between typhoons as long as the typhoons that can affect the YRD.~~ Transport of precursors,
 572 downward airflows, high temperature and light wind are crucial factors, and ~~how big~~ the roles of
 573 those factors play in O₃ episodes depends on behaviors of the typhoons and geographical locations
 574 ~~of the cities~~ typhoon and city. ~~Q~~ It is hard to quantify these processes with just a few cases is a large
 575 ~~challenge.~~ For example, ~~it is hard to find out~~ we cannot estimate whether the downward airflows are
 576 ~~modulated~~ dominated by the subtropical high or the periphery circulation of typhoons since they
 577 usually occur simultaneously. Furthermore, the behave of particulate matter is intriguing since high-
 578 level PM_{2.5} often occurs with high-level O₃ after typhoon, which is opposite to the suggestion
 579 ~~different from previous studies~~ that high particulate matter concentrations inhibit the formation of

O₃ [in previous studies](#) (Li et al., 2005; Xing et al., 2017). This may be related to the heterogeneous reactions (Lou et al., 2014) but research on this issue is quite limited to date.

3.3 Premature mortalities induced by O₃ exposure

When it comes to typhoons, especially landfall typhoons, the first concern is the huge damage caused by extreme weathers. After [the passing of](#) typhoons, people are relieved and [go back busy](#) with their [lifework](#) as usual. However, our research indicates that high O₃ episodes are likely to occur in the short period after a typhoon [landing](#) in the YRD, and high O₃ concentrations can do harm to people's health. To arouse attention on this issue, we estimate the premature mortality attributed to O₃ for respiratory disease, we choose two complete cycles, which is the period A1A3 (21 July to 11 August), to do the calculation. [In this study, we employ the standard damage function defined by epidemiology studies \(Anenverg et al., 2010; Voorhees et al., 2014\) to calculate the premature mortalities due to O₃ exposure, the specific formulas and parameters are described in Section 2.7.](#) Table 4 summarized the premature mortalities in cities in the YRD. The premature mortalities are a function of both the population and O₃ levels, resulting in high premature mortalities in populated and heavily polluted areas. Out of the 26 cities in the YRD, Shanghai [shows](#) highest premature mortalities (29.2) due to its high surface O₃ concentrations and huge population. The city with the lowest premature mortalities (0.6) [was](#) Zhoushan, which may be related to removing effect of the maritime air masses as Zhoushan is located by the sea (Figure 1b). During this period, the total premature mortalities in the YRD [was](#) 194.0, which [was](#) larger than the number of casualties caused directly by the typhoons (80 people were killed by landfall typhoons in mainland China in 2018).

Table 4. Premature mortalities induced by O₃ exposure for respiratory disease

	City	Population (thousand)	Premature mortalities
Category I cities	Shanghai	24,240	29.2
	Yancheng	7,200	6.1
	Nantong	7,310	7.9
	Jiaying	4,726	7.3
	Ningbo	8,202	8.1
	Zhoushan	1,173	0.6

	Taizhou	6,139	4.1
Category II cities	Hangzhou	9,806	16.5
	Taizhoushi	4,636	5.2
	Changzhou	4,729	4.4
	Wuxi	6,575	10.7
	Suzhou	10,722	15.3
	Huzhou	3,027	2.8
	Shaoxing	5,035	4.7
	Jinhua	5,604	8.2
Category III cities	Nanjing	8,436	13.4
	Yangzhou	4,531	5.5
	Zhenjiang	3,196	5.3
	Chuzhou	4,114	5.8
	Maanshan	2,337	3.6
	Wuhu	3,748	6.2
	Xuancheng	2,648	2.0
	Category IV cities	Hefei	8,087
Tongling		1,629	1.7
Chizhou		1,475	2.1
Anqing		4,691	6.4
Total	154,016	194.0	

604

605 4 Conclusions

606 In this study, we investigate the detail processes of landfall typhoons affecting O₃ in the YRD
607 based on a unique case ~~from during~~ 16 July to 25 August, 2018, ~~using both with the help of~~
608 monitoring observations and numerical simulations. This case was characterized by two multiday
609 regional O₃ pollution episodes ~~involving concerned with~~ four successive landfall typhoons. The two
610 O₃ episodes appeared from 24 July to 2 August and 5 to 11 August, respectively, with the highest
611 MDA8 O₃ reached up 264 μg m⁻³.

612 The ~~time when a moment that~~ typhoon reaches the 24-h warning line and the ~~time when the~~
613 ~~last moment of~~ typhoon ~~dies away activity~~ in the mainland China ~~are are~~ crucial, because O₃ pollution
614 episodes mainly occurred during the period from the end of a typhoon ~~to and~~ the arrival of the next
615 typhoon in the YRD. These two moments can be roughly regarded as time nodes. Furthermore, it is
616 found that the variations of O₃ was related to the track, duration and landing intensity of the typhoons
617 during the study period. O₃ pollution ~~first~~ appeared in ~~cities along the coastline coastal region was~~

618 ~~ahead of that in inland regions due to~~along the track of the typhoons. The interval between two
619 typhoons can affect the duration of high O₃ concentration in the YRD. Generally, sustained high O₃
620 concentration ~~– likely appeared in the region on days when the existing typhoon had dissipated~~
621 ~~before the arrival of the next one~~tends to appear on days when the typhoon has dissipated but not
622 ~~influenced by the new one.~~ Regarding the impact of ~~As for~~ the landing intensity of typhoon, the
623 stronger the typhoon landed, the gale and precipitation accompanying the typhoon ~~would~~ be more
624 effective in ~~suppressing O₃ generation~~removing O₃, resulting in lower O₃ concentration in the
625 typhoon landing location.

626 The detail processes of landfall typhoons affecting O₃ depend on typhoons and cities. High
627 temperature and downward airflows ~~dominated by the subtropical high~~ combined with abundant
628 precursors are the main reasons for high O₃ concentration in the YRD in summer. And landfall
629 typhoons can change this state through the following mechanism: When the landfall typhoon is
630 close enough (~ 24-hour warning line), the prevailing southeast wind will change to southwest wind,
631 which transports large amount of precursors from inland to the YRD. The southwest wind usually
632 appears first in coastal regions, and the wind direction will turn ~~back~~ to southeast ~~wind~~ as long as
633 the YRD is dominated by the subtropical high. Then the typhoon makes landfall, the low
634 temperature, precipitation (upward airflows) and wild wind suppress the generation of O₃. After the
635 typhoon passing, the atmosphere ~~in~~at low layers (below 700 hPa) will be warm and dry, and
636 downward airflows resume. The troposphere is likely to fill with high concentration of O₃ due to
637 O₃-rich air transported from the low stratosphere and strong photochemical reactions ~~begin to~~
638 ~~produce O₃ under the abundance of precursors due to foreign sources superposed with local~~
639 ~~emissions.~~ O₃ is mainly generated in the middle of boundary layer (~ 1000 m) instead of at the
640 surface. The high-level O₃ can remain in the residual layer at night, and can be then transported to
641 the surface by downward airflows or turbulent mixing by the second day. The downward airflows
642 also obstruct the vertical diffusion of O₃. Meanwhile, wind speed is light when the wind readjusts
643 to southeast, which further ~~reduces~~worsens horizontal diffusion of O₃. ~~Thus, The~~ O₃ can be
644 accumulated and trapped on the ground. The thermal-dynamic effects results in high surface O₃
645 concentration in the YRD. Those processes will repeat if the next typhoon approaches.

646 The estimated premature mortalities attributed to O₃ exposure for respiratory disease in the
647 YRD during 21 July to 11 August (two complete cycles of typhoons) ~~was~~is 194.0, which is larger

648 than the number of casualties caused directly by the typhoons. This work ~~has~~ enhanced our
649 understanding of how landfall typhoons affect O₃ in the YRD, which may help ~~synthetically~~
650 forecast ~~the~~ O₃ pollution ~~modulated~~~~synthetically~~ ~~impacted~~ by the subtropical high and typhoons.
651 Meanwhile, our results further confirm that large-scale synoptic weather systems play an important
652 role in regional air pollution, suggesting a need in establishing potential links between air pollution
653 and predominant synoptic weather patterns.

654
655 **Author contributions.** C. C. Zhan and M. Xie had the original ideas, designed the research, collected
656 the data, and prepared the original draft. C. C. Zhan carried out the data analysis. M. Xie acquired
657 financial support for the project leading to this publication. C. W. Huang taught and helped C. C.
658 Zhan to do the numerical simulation. J. Liu and T. J. Wang ~~and J. Liu~~ revised the manuscript and
659 helped to collect the data. C. Q. Ma helped to deal with the emission inventory. M. Xu and J. W. Yu
660 helped to collect the data. M. M. Li, S. Li, B. L. Zhuang, and M. Zhao reviewed the initial draft and
661 checked the English of the original manuscript. Y. M. Jiao and D. Y. Nie reviewed the initial draft
662 and helped to improve the work of health impact.

663 664 **Acknowledgements.**

665 This work was supported by the National Key Research and Development Program of China
666 (2018YFC0213502, 2018YFC1506404), the open research fund of Chongqing Meteorological
667 Bureau (KFJJ-201607) and the Fundamental Research Funds for the Central Universities
668 (020714380047).

669 670 **References**

- 671 Allen, R. J., Sherwood, S. C., Norris, J. R., and Zender, C. S.: Recent Northern Hemisphere tropical
672 expansion primarily driven by black carbon and tropospheric ozone, *Nature*, 485, 350-354,
673 10.1038/nature11097, 2012.
- 674 Anenberg, S. C., Horowitz, L. W., Tong, D. Q., and West, J. J.: An estimate of the global burden of
675 anthropogenic ozone and fine particulate matter on premature human mortality using
676 atmospheric modeling, *Environ Health Perspect*, 118, 1189-1195, 10.1289/ehp.0901220, 2010.
- 677 Burnett, R. T., Pope, C. A., 3rd, Ezzati, M., Olives, C., Lim, S. S., Mehta, S., Shin, H. H., Singh, G.,

678 Hubbell, B., Brauer, M., Anderson, H. R., Smith, K. R., Balme, J. R., Bruce, N. G., Kan, H.,
679 Laden, F., Pruss-Ustun, A., Turner, M. C., Gapstur, S. M., Diver, W. R., and Cohen, A.: An
680 integrated risk function for estimating the global burden of disease attributable to ambient fine
681 particulate matter exposure, *Environ Health Perspect*, 122, 397-403, 10.1289/ehp.1307049,
682 2014.

683 Chameides, W., and Walker, J. C. G.: A photochemical theory of tropospheric ozone, *Journal of*
684 *Geophysical Research*, 78, 8751-8760, 10.1029/JC078i036p08751, 1973.

685 Chan, C. K., and Yao, X.: Air pollution in mega cities in China, *Atmospheric Environment*, 42, 1-
686 42, 10.1016/j.atmosenv.2007.09.003, 2008.

687 Deng, T., Wang, T., Wang, S., Zou, Y., Yin, C., Li, F., Liu, L., Wang, N., Song, L., Wu, C., and Wu,
688 D.: Impact of typhoon periphery on high ozone and high aerosol pollution in the Pearl River
689 Delta region, *The Science of the total environment*, 668, 617-630,
690 10.1016/j.scitotenv.2019.02.450, 2019.

691 Ding, A. J., Wang, T., Thouret, V., Cammas, J. P., and Nedelec, P.: Tropospheric ozone climatology
692 over Beijing: analysis of aircraft data from the MOZAIC program, *Atmospheric Chemistry and*
693 *Physics*, 8, 1-13, 2008.

694 Ding, A. J., Fu, C. B., Yang, X. Q., Sun, J. N., Zheng, L. F., Xie, Y. N., Herrmann, E., Nie, W., Petäjä,
695 T., Kerminen, V. M., and Kulmala, M.: Ozone and fine particle in the western Yangtze River
696 Delta: an overview of 1 yr data at the SORPES station, *Atmospheric Chemistry and Physics*,
697 13, 5813-5830, 10.5194/acp-13-5813-2013, 2013.

698 Ding, A., Nie, W., Huang, X., Chi, X., Sun, J., Kerminen, V.-M., Xu, Z., Guo, W., Petäjä, T., Yang,
699 X., Kulmala, M., and Fu, C.: Long-term observation of air pollution-weather/climate
700 interactions at the SORPES station: a review and outlook, *Frontiers of Environmental Science*
701 *& Engineering*, 10, 10.1007/s11783-016-0877-3, 2016.

702 Dong J Y, Liu X R, Zhang B Z.: Meta-analysis of association between short-term ozone exposure
703 and population mortality in China, *Acta Scientiae Circumstantiae*, 36 (4), 1477-1485, 2016 (in
704 Chinese).

705 Fan, Q., Lan, J., Liu, Y. M., Wang, X. M., Chan, P. W., Hong, Y. Y., Feng, Y. R., Liu, Y. X., Zeng, Y.
706 J., and Liang, G. X.: Process analysis of regional aerosol pollution during spring in the Pearl
707 River Delta region, China, *Atmospheric Environment*, 122, 829-838, 2015.

708 Ghude, S. D., Chate, D. M., Jena, C., Beig, G., Kumar, R., Barth, M. C., Pfister, G. G., Fadnavis, S.,
709 and Pithani, P.: Premature mortality in India due to PM_{2.5} and ozone exposure, *Geophys Res*
710 *Lett*, 43, 4650-4658, 10.1002/2016gl068949, 2016.

711 Guo, S., Hu, M., Zamora, M. L., Peng, J., Shang, D., Zheng, J., Du, Z., Wu, Z., Shao, M., Zeng, L.,
712 Molina, M. J., and Zhang, R.: Elucidating severe urban haze formation in China, *Proceedings*
713 *of the National Academy of Sciences of the United States of America*, 111, 17373-17378,
714 10.1073/pnas.1419604111, 2014.

715 Hu, J., Chen, J., Ying, Q., and Zhang, H.: One-year simulation of ozone and particulate matter in
716 China using WRF/CMAQ modeling system, *Atmospheric Chemistry and Physics*, 16, 10333-
717 10350, 10.5194/acp-16-10333-2016, 2016.

718 Huang, J.-P.: Numerical simulation and process analysis of typhoon-related ozone episodes in Hong
719 Kong, *Journal of Geophysical Research*, 110, 10.1029/2004jd004914, 2005.

720 Huang, R. J., Zhang, Y., Bozzetti, C., Ho, K. F., Cao, J. J., Han, Y., Daellenbach, K. R., Slowik, J.
721 G., Platt, S. M., Canonaco, F., Zotter, P., Wolf, R., Pieber, S. M., Bruns, E. A., Crippa, M.,
722 Ciarelli, G., Piazzalunga, A., Schwikowski, M., Abbaszade, G., Schnelle-Kreis, J.,
723 Zimmermann, R., An, Z., Szidat, S., Baltensperger, U., El Haddad, I., and Prevot, A. S.: High
724 secondary aerosol contribution to particulate pollution during haze events in China, *Nature*,
725 514, 218-222, 10.1038/nature13774, 2014.

726 Jerrett, M., Burnett, R. T., Pope, C. A., Ito, K., Thurston, G., Krewski, D., Shi, Y. L., Calle, E., and
727 Thun, M.: Long-Term Ozone Exposure and Mortality., *New Engl J Med*, 360, 1085-1095, 2009.

728 [Jiang, Y. C., Zhao, T. L., Liu, J., Xu, X. D., Tan, C. H., Cheng, X. H., Bi, X. Y., Gan, J. B., You, J.](#)
729 [F., and Zhao, S. Z.: Why does surface ozone peak before a typhoon landing in southeast China?,](#)
730 [Atmospheric Chemistry and Physics, 15, 13331-13338, 10.5194/acp-15-13331-2015, 2015.](#)

731 Jiménez, P. A., and Dudhia, J.: Improving the Representation of Resolved and Unresolved
732 Topographic Effects on Surface Wind in the WRF Model, *Journal of Applied Meteorology and*
733 *Climatology*, 51, 300-316, 10.1175/jamc-d-11-084.1, 2012.

734 Jin, Y., Andersson, H., and Zhang, S.: Air Pollution Control Policies in China: A Retrospective and
735 Prospects, *Int J Environ Res Public Health*, 13, 10.3390/ijerph13121219, 2016.

736 Kamens, R., Jang, M., Chien, C. J., and Leach, K.: Aerosol formation from the reaction of alpha-
737 pinene and ozone using a gas-phase kinetics aerosol partitioning model, *Environmental*

738 Science & Technology, 33, 1430-1438, 1999.

739 Kan, H., Chen, R., and Tong, S.: Ambient air pollution, climate change, and population health in
740 China, *Environ Int*, 42, 10-19, 10.1016/j.envint.2011.03.003, 2012.

741 Khoder, M. I.: Atmospheric conversion of sulfur dioxide to particulate sulfate and nitrogen dioxide
742 to particulate nitrate and gaseous nitric acid in an urban area, *Chemosphere*, 49, 675-684, 2002.

743 Lelieveld, J., Evans, J. S., Fnais, M., Giannadaki, D., and Pozzer, A.: The contribution of outdoor
744 air pollution sources to premature mortality on a global scale, *Nature*, 525, 367-371,
745 10.1038/nature15371, 2015.

746 Li, L., Chen, C. H., Fu, J. S., Huang, C., Streets, D. G., Huang, H. Y., Zhang, G. F., Wang, Y. J.,
747 Jang, C. J., Wang, H. L., Chen, Y. R., and Fu, J. M.: Air quality and emissions in the Yangtze
748 River Delta, China, *Atmospheric Chemistry and Physics*, 11, 1621-1639, 10.5194/acp-11-
749 1621-2011, 2011.

750 Li, L., Chen, C. H., Huang, C., Huang, H. Y., Zhang, G. F., Wang, Y. J., Wang, H. L., Lou, S. R.,
751 Qiao, L. P., Zhou, M., Chen, M. H., Chen, Y. R., Streets, D. G., Fu, J. S., and Jang, C. J.: Process
752 analysis of regional ozone formation over the Yangtze River Delta, China using the Community
753 Multi-scale Air Quality modeling system, *Atmospheric Chemistry and Physics*, 12, 10971-
754 10987, 2012.

755 Li, S. H., and Hong, H. P.: Typhoon wind hazard estimation for China using an empirical track
756 model, *Natural Hazards*, 82, 1009-1029, 10.1007/s11069-016-2231-2, 2016.

757 Li, M., Liu, H., Geng, G., Hong, C., Liu, F., Song, Y., Tong, D., Zheng, B., Cui, H., Man, H., Zhang,
758 Q., and He, K.: Anthropogenic emission inventories in China: a review, *National Science*
759 *Review*, 4, 834-866, 10.1093/nsr/nwx150, 2017.

760 Li, M., Wang, T., Xie, M., Zhuang, B., Li, S., Han, Y., and Chen, P.: Impacts of aerosol-radiation
761 feedback on local air quality during a severe haze episode in Nanjing megacity, eastern China,
762 *Tellus B: Chemical and Physical Meteorology*, 69, 10.1080/16000889.2017.1339548, 2017.

763 Li, M., Wang, T., Xie, M., Zhuang, B., Li, S., Han, Y., Song, Y., and Cheng, N.: Improved
764 meteorology and ozone air quality simulations using MODIS land surface parameters in the
765 Yangtze River Delta urban cluster, China, *Journal of Geophysical Research: Atmospheres*, 122,
766 3116-3140, 10.1002/2016jd026182, 2017.

767 Li, S., Wang, T., Huang, X., Pu, X., Li, M., Chen, P., Yang, X.-Q., and Wang, M.: Impact of East

768 Asian Summer Monsoon on Surface Ozone Pattern in China, *Journal of Geophysical Research:*
769 *Atmospheres*, 123, 1401-1411, 10.1002/2017jd027190, 2018.

770 Li, M., Wang, T., Xie, M., Li, S., Zhuang, B., Huang, X., Chen, P., Zhao, M., and Liu, J.: Formation
771 and Evolution Mechanisms for Two Extreme Haze Episodes in the Yangtze River Delta Region
772 of China During Winter 2016, *Journal of Geophysical Research: Atmospheres*, 124, 3607-3623,
773 10.1029/2019jd030535, 2019.

774 Liao, J., Wang, T., Jiang, Z., Zhuang, B., Xie, M., Yin, C., Wang, X., Zhu, J., Fu, Y., and Zhang, Y.:
775 WRF/Chem modeling of the impacts of urban expansion on regional climate and air pollutants
776 in Yangtze River Delta, China, *Atmospheric Environment*, 106, 204-214,
777 10.1016/j.atmosenv.2015.01.059, 2015.

778 Liao, Z., Gao, M., Sun, J., and Fan, S.: The impact of synoptic circulation on air quality and
779 pollution-related human health in the Yangtze River Delta region, *The Science of the total*
780 *environment*, 607-608, 838-846, 10.1016/j.scitotenv.2017.07.031, 2017.

781 Liu, D., Pang, L., and Xie, B.: Typhoon disaster in China: prediction, prevention, and mitigation,
782 *Natural Hazards*, 49, 421-436, 10.1007/s11069-008-9262-2, 2009.

783 Liu, H., Liu, S., Xue, B. R., Lv, Z. F., Meng, Z. H., Yang, X. F., Xue, T., Yu, Q., and He, K. B.:
784 Ground-level ozone pollution and its health impacts in China, *Atmospheric Environment*, 173,
785 223-230, 2018.

786 Lou, S., Liao, H., and Zhu, B.: Impacts of aerosols on surface-layer ozone concentrations in China
787 through heterogeneous reactions and changes in photolysis rates, *Atmospheric Environment*,
788 85, 123-138, 10.1016/j.atmosenv.2013.12.004, 2014.

789 Lu, X., Hong, J., Zhang, L., Cooper, O. R., Schultz, M. G., Xu, X., Wang, T., Gao, M., Zhao, Y., and
790 Zhang, Y.: Severe Surface Ozone Pollution in China: A Global Perspective, *Environmental*
791 *Science & Technology Letters*, 5, 487-494, 10.1021/acs.estlett.8b00366, 2018.

792 Monks, P. S., Archibald, A. T., Colette, A., Cooper, O., Coyle, M., Derwent, R., Fowler, D., Granier,
793 C., Law, K. S., Mills, G. E., Stevenson, D. S., Tarasova, O., Thouret, V., von Schneidmesser,
794 E., Sommariva, R., Wild, O., and Williams, M. L.: Tropospheric ozone and its precursors from
795 the urban to the global scale from air quality to short-lived climate forcer, *Atmospheric*
796 *Chemistry and Physics*, 15, 8889-8973, 10.5194/acp-15-8889-2015, 2015.

797 Shu, L., Xie, M., Wang, T., Gao, D., Chen, P., Han, Y., Li, S., Zhuang, B., and Li, M.: Integrated

798 studies of a regional ozone pollution synthetically affected by subtropical high and typhoon
799 system in the Yangtze River Delta region, China, *Atmospheric Chemistry and Physics*, 16,
800 15801-15819, 10.5194/acp-16-15801-2016, 2016.

801 Shu, L., Xie, M., Gao, D., Wang, T., Fang, D., Liu, Q., Huang, A., and Peng, L.: Regional severe
802 particle pollution and its association with synoptic weather patterns in the Yangtze River Delta
803 region, China, *Atmospheric Chemistry and Physics*, 17, 12871-12891, 10.5194/acp-17-12871-
804 2017, 2017.

805 Tang, X.Y., Li, J.L., Dong, Z.X., Wang, Y.Y., Wang, W.X., Qi, L.W., Liu, X.L., Zhang, Y.T., Zhang,
806 X.J., Tian, B.S., Jin, S.W., Yang, L.Q., Zhang, Y.X., 1989. Photochemical pollution in Lanzhou,
807 China - a case study. *J. Environ. Sci. China* 1, 31e38.

808 Van Dingenen, R., Dentener, F. J., Raes, F., Krol, M. C., Emberson, L., and Cofala, J.: The global
809 impact of ozone on agricultural crop yields under current and future air quality legislation,
810 *Atmospheric Environment*, 43, 604-618, 10.1016/j.atmosenv.2008.10.033, 2009.

811 Voorhees, A. S., Wang, J., Wang, C., Zhao, B., Wang, S., and Kan, H.: Public health benefits of
812 reducing air pollution in Shanghai: a proof-of-concept methodology with application to
813 BenMAP, *The Science of the total environment*, 485-486, 396-405,
814 10.1016/j.scitotenv.2014.03.113, 2014.

815 Wang, T., and Kwok, J. Y. H.: Measurement and analysis of a multiday photochemical smog episode
816 in the Pearl River delta of China, *J Appl Meteorol*, 42, 404-416, 2003.

817 Wang, X., Zhang, Y., Hu, Y., Zhou, W., Lu, K., Zhong, L., Zeng, L., Shao, M., Hu, M., and Russell,
818 A. G.: Process analysis and sensitivity study of regional ozone formation over the Pearl River
819 Delta, China, during the PRIDE-PRD2004 campaign using the Community Multiscale Air
820 Quality modeling system, *Atmospheric Chemistry and Physics*, 10, 4423-4437, 10.5194/acp-
821 10-4423-2010, 2010.

822 Wang, M., Cao, C., Li, G., and Singh, R. P.: Analysis of a severe prolonged regional haze episode
823 in the Yangtze River Delta, China, *Atmospheric Environment*, 102, 112-121,
824 10.1016/j.atmosenv.2014.11.038, 2015.

825 Wang, T., Xue, L., Brimblecombe, P., Lam, Y. F., Li, L., and Zhang, L.: Ozone pollution in China:
826 A review of concentrations, meteorological influences, chemical precursors, and effects, *The
827 Science of the total environment*, 575, 1582-1596, 10.1016/j.scitotenv.2016.10.081, 2017.

828 Wang, T., Gao, T., Zhang, H., Ge, M., Lei, H., Zhang, P., Zhang, P., Lu, C., Liu, C., Zhang, H.,
829 Zhang, Q., Liao, H., Kan, H., Feng, Z., Zhang, Y., Qie, X., Cai, X., Li, M., Liu, L., and Tong,
830 S.: Review of Chinese atmospheric science research over the past 70 years: Atmospheric
831 physics and atmospheric environment, *Science China Earth Sciences*, 62, 1903-1945,
832 10.1007/s11430-019-9536-1, 2019.

833 Wei, X., Lam, K.-s., Cao, C., Li, H., and He, J.: Dynamics of the Typhoon Haitang Related High
834 Ozone Episode over Hong Kong, *Advances in Meteorology*, 2016, 1-12,
835 10.1155/2016/6089154, 2016.

836 Xie, M., Zhu, K., Wang, T., Yang, H., Zhuang, B., Li, S., Li, M., Zhu, X., and Ouyang, Y.:
837 Application of photochemical indicators to evaluate ozone nonlinear chemistry and pollution
838 control countermeasure in China, *Atmospheric Environment*, 99, 466-473,
839 10.1016/j.atmosenv.2014.10.013, 2014.

840 Xie, M., Liao, J., Wang, T., Zhu, K., Zhuang, B., Han, Y., Li, M., and Li, S.: Modeling of the
841 anthropogenic heat flux and its effect on regional meteorology and air quality over the Yangtze
842 River Delta region, China, *Atmospheric Chemistry and Physics*, 16, 6071-6089, 10.5194/acp-
843 16-6071-2016, 2016.

844 Xie, M., Zhu, K., Wang, T., Chen, P., Han, Y., Li, S., Zhuang, B., and Shu, L.: Temporal
845 characterization and regional contribution to O₃ and NO_x at an urban and a suburban site in
846 Nanjing, China, *The Science of the total environment*, 551-552, 533-545,
847 10.1016/j.scitotenv.2016.02.047, 2016.

848 Xie, M., Shu, L., Wang, T.-j., Liu, Q., Gao, D., Li, S., Zhuang, B.-l., Han, Y., Li, M.-m., and Chen,
849 P.-l.: Natural emissions under future climate condition and their effects on surface ozone in the
850 Yangtze River Delta region, China, *Atmospheric Environment*, 150, 162-180,
851 10.1016/j.atmosenv.2016.11.053, 2017.

852 Xu, X., Lin, W., Wang, T., Yan, P., Tang, J., Meng, Z., and Wang, Y.: Long-term trend of surface
853 ozone at a regional background station in eastern China 1991-2006: enhanced variability,
854 *Atmospheric Chemistry and Physics*, 8, 2595-2607, 2008.

855 Xue, L. K., Wang, T., Gao, J., Ding, A. J., Zhou, X. H., Blake, D. R., Wang, X. F., Saunders, S. M.,
856 Fan, S. J., Zuo, H. C., Zhang, Q. Z., and Wang, W. X.: Ground-level ozone in four Chinese
857 cities: precursors, regional transport and heterogeneous processes, *Atmospheric Chemistry and*

858 Physics, 14, 13175-13188, 10.5194/acp-14-13175-2014, 2014.

859 Yang, J. X., Lau, A. K. H., Fung, J. C. H., Zhou, W., and Wenig, M.: An air pollution episode and
860 its formation mechanism during the tropical cyclone Nuri's landfall in a coastal city of south
861 China, *Atmospheric Environment*, 54, 746-753, 10.1016/j.atmosenv.2011.12.023, 2012.

862 Ying, M., Zhang, W., Yu, H., Lu, X., Feng, J., Fan, Y., Zhu, Y., and Chen, D.: An Overview of the
863 China Meteorological Administration Tropical Cyclone Database, *Journal of Atmospheric and*
864 *Oceanic Technology*, 31, 287-301, 10.1175/jtech-d-12-00119.1, 2014.

865 Zhan, C.-c., Xie, M., Fang, D.-x., Wang, T.-j., Wu, Z., Lu, H., Li, M.-m., Chen, P.-l., Zhuang, B.-l.,
866 Li, S., Zhang, Z.-q., Gao, D., Ren, J.-y., and Zhao, M.: Synoptic weather patterns and their
867 impacts on regional particle pollution in the city cluster of the Sichuan Basin, China,
868 *Atmospheric Environment*, 208, 34-47, 10.1016/j.atmosenv.2019.03.033, 2019.

869 Zhang, Q. A., Wu, L. G., and Liu, Q. F.: Tropical Cyclone Damages in China 1983-2006, *Bulletin*
870 *of the American Meteorological Society*, 90, 489-+, 2009.

871 Zhao, C., Wang, Y., Yang, Q., Fu, R., Cunnold, D., and Choi, Y.: Impact of East Asian summer
872 monsoon on the air quality over China: View from space, *Journal of Geophysical Research*,
873 115, 10.1029/2009jd012745, 2010.

874 Zhao, K., Li, X., Xue, M., Jou, B. J.-D., and Lee, W.-C.: Short-term forecasting through intermittent
875 assimilation of data from Taiwan and mainland China coastal radars for Typhoon Meranti
876 (2010) at landfall, *Journal of Geophysical Research: Atmospheres*, 117, n/a-n/a,
877 10.1029/2011jd017109, 2012.

878